applied sciences

MDPI

Article

New 3-(6-Bromo-2-oxo-1,3-benzoxazol-3(2*H*)-yl)propanoic Acid Derivatives: Synthesis and Biological Activity Against Bacterial Pathogens

Monika Bertašiūtė [1], Jūratė Šiugždaitė [2], Birutė Grybaitė [1], Birutė Sapijanskaitė-Banevič [1], Livija Tubytė [2], Raimundas Lelešius [2], Sergey Belyakov [3], Mindaugas Marksa [4], Andrejus Ževžikovas [4] and Vytautas Mickevičius [1,*]

[1] Department of Organic Chemistry, Kaunas University of Technology, Radvilėnų Road 19, 50254 Kaunas, Lithuania
[2] Department of Veterinary Pathobiology, Lithuanian University of Health Sciences, Tilžės Street 18, 47181 Kaunas, Lithuania; livija.tubyte@lsmu.lt (L.T.); raimundas.lelesius@lsmu.lt (R.L.)
[3] Laboratory of Physical Organic Chemistry, Latvian Institute of Organic Synthesis, Aizkraukles St. 21, LV-1006 Riga, Latvia
[4] Department of Analytical and Toxicological Chemistry, Lithuanian University of Health Sciences, Sukilėlių pr. 13, 50162 Kaunas, Lithuania
* Correspondence: vytautas.mickevicius@ktu.lt

Abstract

Continuing our work in the field of synthesis and research of amino acids, their derivatives, and cyclization products, in this work, we synthesized various 3-(6-bromo-2-oxo-1,3-benzoxazol-3(2*H*)-yl)propanoic acid derivatives and investigated their antimicrobial activity. A total of eighteen synthesized chemical compounds (No. **1–18**), including several structural analogues (e.g., **3a**, **3b**, **4a–4e**, **8a–8m**, **9a–9d**), were evaluated for their antibacterial properties. The antibacterial activity was assessed using the Kirby–Bauer disk diffusion method, and inhibition zone diameters (mm) were measured against five representative bacterial strains: *S. aureus*, *MRSA*, *B. subtilis*, *E. coli*, and *P. aeruginosa*. The minimum inhibitory concentrations (MICs) and minimum bactericidal concentrations (MBCs) of the most active synthesized compounds were determined against representative Gram-positive and Gram-negative bacterial strains, including *S. aureus*, *MRSA*, *B. subtilis*, and *E. coli*. Overall, these results indicate that the tested compounds display selective antibacterial activity, mainly against Gram-positive bacteria, with compound **12** emerging as the most promising derivative in the series. The antibacterial activities of several synthesized compounds were systematically evaluated against *S. aureus* and MRSA over a 24 h incubation period, with optical density measured at ten time points. Bacterial growth was monitored spectrophotometrically at 600 nm (OD_{600}) at 1, 2, 3, 4, 5, 6, 7, 8, 20, and 24 h, enabling a detailed assessment of growth kinetics and the temporal dynamics of inhibition. The effect of compound **11** on the growth kinetics of S. aureus was evaluated by quantifying viable bacterial counts ($\log_{10}$ CFU/mL) over a 6 h incubation period, and the results are presented in the time–kill curve. Compound **11** was selected for this experiment because it exhibited the most pronounced antibacterial activity against S. aureus in the disk diffusion assay. The cytotoxicity of compounds **9a**, **11**, **12**, and **13** was evaluated at concentrations ranging from 125 to 1.95 μg/mL. The results showed a clear, concentration-dependent decrease in cytotoxicity for all tested compounds. The molecular structure of compound **3a** was confirmed by a single-crystal X-ray diffraction.

Academic Editor: Samuel Adeloju

Received: 7 January 2026
Revised: 30 January 2026
Accepted: 17 February 2026
Published: 21 February 2026

Keywords: 3-(6-Bromobenzoxazolonyl-3)propanoic acid; hydrazones; azoles; antibacterial activity

1. Introduction

Benzoxazoles represent an important class of fused heterocycles, consisting of a benzene ring fused to an oxazole nucleus. Their compact, planar architecture, enriched with heteroatoms, enables multiple modes of molecular recognition, such as π–π stacking, hydrogen bonding, and metal coordination [1–3]. These properties, together with their occurrence in natural products such as UK-1 (**I**) and caboxamycin (**II**), have made benzoxazoles a privileged scaffold in medicinal chemistry [2,4] (Figure 1).

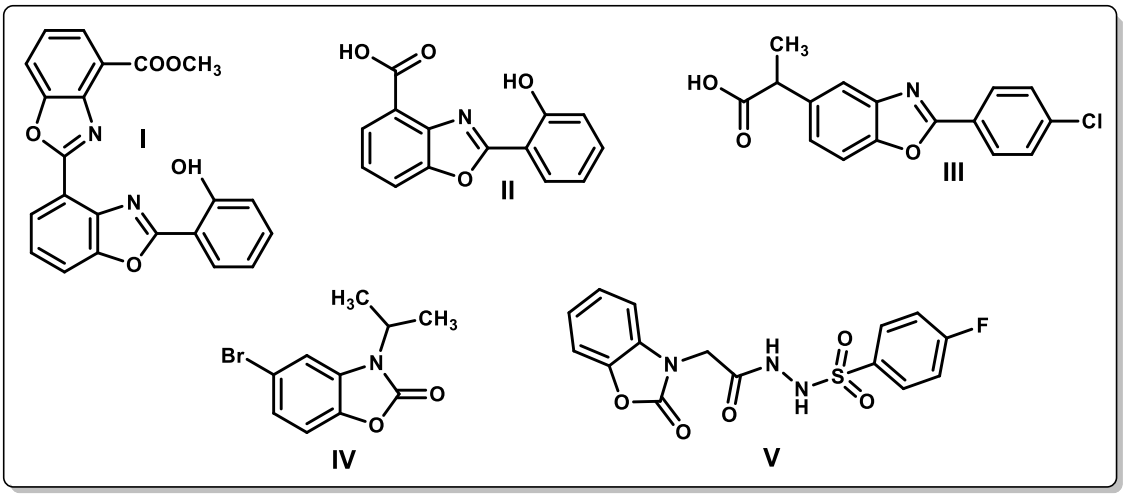

Figure 1. Structures of biologically active benzoxazole derivatives.

Over the past decades, benzoxazole derivatives have been reported to exhibit an impressive diversity of biological activities. They have demonstrated potent antibacterial effects against both Gram-positive and Gram-negative pathogens, including *Staphylococcus aureus* and *Enterococcus* species, and some compounds have emerged as promising leads against *Mycobacterium* species, including *Mycobacterium tuberculosis* [5–14]. For example, structure **III** is a nonsteroidal anti-inflammatory agent marketed as an antirheumatic drug [10]. Compound **IV** exhibits anticancer properties [14], and molecule **V** reduces paraoxonase-1 enzyme activity at very low concentrations [12]. In addition, benzoxazoles have displayed antiviral activity [15,16].

The search for new chemotypes with novel mechanisms of action [17]. Multidrug-resistant (MDR) pathogens, including methicillin-resistant *Staphylococcus aureus* (MRSA) and Pseudomonas aeruginosa, pose significant clinical challenges, resulting in increased morbidity, mortality, and healthcare costs. [18]. The alarming rise in resistance rates has outpaced the discovery of new antibiotic classes, emphasizing the need for innovative approaches to antimicrobial drug design [19].

Beyond their anti-infective properties, benzoxazoles are recognized for their anticancer potential. Numerous analogues induce apoptosis, inhibit poly(ADP-ribose) polymerase (PARP-2), modulate kinases such as VEGFR-2, or act as monoacylglycerol lipase (MAGL) inhibitors, resulting in cytotoxicity against a wide spectrum of cancer cell lines [20–32].

Other reported activities further underscore the pharmacological versatility of this scaffold. Benzoxazole derivatives have been investigated as anti-inflammatory and analgesic agents through enzyme inhibition pathways [32–41], while others display activity as

allosteric modulators of metabolic enzymes and as antagonists of neurotransmitter receptors [42–45]. Promising leads have also been reported as antiparasitic agents, expanding the relevance of benzoxazoles beyond classical therapeutic areas [46].

2. Materials and Methods

2.1. General Information

Reagents and solvents were obtained from Sigma–Aldrich (St. Louis, MO, USA) and used without further purification. The reaction course and purity of the synthesized compounds were monitored by TLC using aluminium plates precoated with Silica gel with F254 nm (Merck KGaA, Darmstadt, Germany). Melting points were determined with a B-540 melting point analyzer (Büchi Corporation, New Castle, DE, USA) and were uncorrected. NMR spectra were recorded on a Bruker Avance III (400, 101 MHz) spectrometer (Bruker BioSpin AG, Fällanden, Switzerland). Chemical shifts were reported in (d) ppm relative to tetramethylsilane (TMS) with the residual solvent as internal reference (DMSO-d_6, d = 2.50 ppm for ^{1}H and d = 39.52 ppm for ^{13}C). Data were reported as follows: chemical shift, multiplicity, coupling constant (Hz), integration, and assignment. IR spectra (ν, cm^{-1}) were recorded on a PerkinElmer Frontier spectrometer (PerkinElmer Inc., Waltham, MA, USA) in a wave interval from 4000 to 560 cm^{-1}, by pressing a small amount of sample against a diamond crystal plate (number of scans—6, resolution—4 cm^{-1}), and data were processed using Spectrum software (version 10.03.03). Mass spectra were recorded on Ms. Agilent 6530A QTOF HPLC, Agilent 1260 II series (Agilent Technologies, Inc., Santa Clara, CA, USA). The C, H, and N elemental analysis was conducted on an Elemental Analyzer CE-440 (Exeter Analytical, Inc., Chelmsford, MA, USA). The results were found to be in good agreement (±0.3%) with the calculated values.

3-(6-bromo-2-oxobenzo[d]oxazol-3(2H)-yl)propanoic acid (**2**)

Carboxylic acid **1** [47] (18.65 g, 90 mmol) was dissolved in acetic acid (60 mL) at 70 °C. After cooling to room temperature, Br_2 (9.3 mL, 180 mmol, dropwise) was added. The mixture was stirred for 4 h, sodium thiosulfate pentahydrate (0.5 g) was added under stirring, then diluted with 300 mL water, and the formed precipitate was filtered off and washed with hot water. The obtained acid **2** was purified by recrystallisation from propan-2-ol.

Light brown solid, yield 23.50 g (91%), m.p. 167–169 °C.

^{1}H NMR (400 MHz, DMSO-d_6), δ: 2.68 (t, J = 6.9 Hz, 2H, CH_2), 4.00 (t, J = 7.0 Hz, 2H, N-CH_2), 7.31 (d, J = 8.3 Hz, 1H, H_{arom}), 7.40 (d, J = 8.4 Hz, 1H, H_{arom}), 7.63 (s, 1H, H_{arom}).

^{13}C NMR (101 MHz, DMSO-d_6), δ: 31.69 ($\underline{C}H_2$-CO), 38.05 (N–CH_2), 111.01, 112.68, 113.24, 126.35, 130.35, 142.42 (C_{arom}), 153.06 (C=O), 172.04 (COOH).

HRMS (ESI): m/z calcd. for $C_{10}H_8BrNO_4$ 309.0810; Found: 309.2500 $[M + Na]^+$.

IR (KBr), ν, cm^{-1}: 3424 (OH), 1769, 1700 (2x C=O).

6-bromo-3-(3-oxo-3-(p-tolyl)propyl)benzo[d]oxazol-2(3H)-one (**3a**)

A mixture of phosphorus pentoxide (5 g) and toluene (50 mL) was heated under reflux for 20 min, after which carboxylic acid **2** (1.43 g, 5 mmol) was added. Reflux was continued for 4 h. Upon completion, the reaction mixture was allowed to cool, and the liquid was decanted from the residue. The liquid was then concentrated under reduced pressure to approximately 1 mL and diluted with hexane (15 mL). The resulting mixture was left to stand at room temperature for 1 day and then at the temperature of 4 °C for 1 day. The formed precipitate was collected by filtration, washed with hexane, and dried. The obtained material **3a** was purified by recrystallisation from a toluene (25 mL) and hexane (25 mL) mixture.

Pale-yellow solid, yield 0.40 g (30%), m.p. 132–134 °C.

^{1}H NMR (400 MHz, DMSO-d_6), δ: 2.36 (s, 3H, CH_3), 3.51 (t, J = 6.9 Hz, 2H, CH_2), 4.14 (t, J = 6.8 Hz, 2H, CH_2), 7.31 (d, J = 7.9 Hz, 2H, H_{arom}), 7.40 (t, J = 6.6 Hz, 2H, H_{arom}), 7.63 (s, 1H, H_{arom}), 7.84 (d, J = 7.8 Hz, 2H, H_{arom}).

^{13}C NMR (101 MHz, DMSO-d_6), δ: 21.16 (CH_3), 35.58 ($\underline{C}H_2$-C), 37.46 (N-CH_2), 111.32, 112.79, 113.37, 126.50, 128.07, 129.26, 130.64, 133.69, 142.62, 143.88 (C_{arom}), 153.26, 197.13 (2x C=O).

HRMS (ESI): m/z calcd. for $C_{17}H_{14}BrNO_3$ 360.0157; Found: 360.0679 $[M + H]^+$.

IR (KBr), ν, cm^{-1} = 1762, 1668 (2x C=O).

6-bromo-3-(3-(3,4-dimethylphenyl)-3-oxopropyl)benzo[d]oxazol-2(3H)-one (**3b**)

A mixture of phosphorus pentoxide (2.5 g), *o*-xylene (25 mL) was heated under reflux for 20 min, after which carboxylic acid **2** (0.72 g, 2.5 mmol) was added. Reflux was continued for 4 h. Upon completion, the reaction mixture was allowed to cool, and the liquid was decanted from the residue. The liquid was then concentrated under reduced pressure to approximately 1 mL and diluted with hexane (15 mL). The resulting mixture was left to stand at room temperature for 1 day and then at a temperature of 4 °C for 1 day. The formed precipitate was collected by filtration, washed with hexane, and dried. The obtained material **3b** was purified by recrystallisation from toluene (25 mL) and hexane (25 mL) mixture.

Pale-yellow solid, yield 0.21 g (23%), m.p. 136–138 °C.

^{1}H NMR (400 MHz, DMSO-d_6), δ: 2.25 (s, 3H, CH_3), 2.27 (s, 3H, CH_3), 3.50 (t, J = 6.8 Hz, 2H, CH_2), 4.14 (t, J = 6.8 Hz, 2H, CH_2), 7.26 (d, J = 7.9 Hz, 1H, H_{arom}), 7.35–7.46 (m, 2H, H_{arom}), 7.60–7.75 (m, 3H, H_{arom}).

^{13}C NMR (101 MHz, DMSO-d_6), δ: 19.30, 19.61 (2x CH_3), 35.61 ($\underline{C}H_2$-CO), 37.51 (N-CH_2), 111.35, 112.80, 113.39, 125.63, 126.52, 128.95, 129.75, 130.65, 134.05, 136.76, 142.63, 142.72 (C_{arom}), 153.27, 197.31 (2x C=O).

HRMS (ESI): m/z calcd. for $C_{18}H_{16}BrNO_3$ 374.0314; Found: 374.0802 $[M + H]^+$.

IR (KBr), ν, cm^{-1} = 1759, 1668 (2x C=O).

General Procedure for Preparation of Benzimidazoles (**4a**–**d**)

A mixture of carboxylic acid **2** (1.72 g, 6 mmol), the corresponding benzene-1,2-diamine (12 mmol), and 18% aqueous hydrochloric acid solution (25 mL) was heated at reflux for 72 h. Afterwards, it was cooled and neutralized with 5% Na_2CO_3 to pH 9. The formed precipitate was filtered off, washed with hot water, and recrystallized from propan-2-ol.

3-(2-(1H-benzo[d]imidazol-2-yl)ethyl)-6-bromobenzo[d]oxazol-2(3H)-one (**4a**)

Brown solid, yield 1.38 g (64%), m.p. 142–144 °C.

^{1}H NMR (400 MHz, DMSO-d_6), δ: 3.23 (d, J = 7.0 Hz, 2H, CH_2), 4.26 (t, J = 6.7 Hz, 2H, CH_2), 7.12 (s, 2H, H_{arom}), 7.20 (d, J = 8.3 Hz, 1H, H_{arom}), 7.33 (d, J = 8.3 Hz, 1H, H_{arom}), 7.45 (s, 2H, H_{arom}), 7.63 (s, 1H, H_{arom}), 12.34 (s, 1H, NH).

^{13}C NMR (101 MHz, DMSO-d_6), δ: 26.85 ($\underline{C}H_2$-CO), 40.60 (N-CH_2), 110.75, 112.94, 113.44, 126.45, 130.47 (C_{arom}), 142.63 (CH_2-$\underline{C}$=N), 153.27 (C=O).

HRMS (ESI): m/z calcd. for $C_{16}H_{12}BrN_3O_2$ 358.0113; Found: 358.0679 $[M + H]^+$.

IR (KBr), ν, cm^{-1} = 2860 (NH), 1770, 1698 (2x C=O), 1615 (C=N).

6-bromo-3-(2-(5-methyl-1H-benzo[d]imidazol-2-yl)ethyl)benzo[d]oxazol-2(3H)-one (**4b**)

Brown solid, yield 1.30 g (58%), m.p. 98–100 °C.

^{1}H NMR (400 MHz, DMSO-d_6), δ: 2.37 (s, 3H, CH_3), 3.20 (t, J = 7.1 Hz, 2H, CH_2), 4.24 (t, J = 6.9 Hz, 2H, CH_2), 6.93 (d, J = 8.1 Hz, 1H, H_{arom}), 7.16–7.39 (m, 4H, H_{arom}), 7.63 (s, 1H, H_{arom}), 12.17 (s, 1H, NH).

^{13}C NMR (101 MHz, DMSO-d_6), δ: 21.70 (CH_3), 26.83 ($\underline{C}H_2$-C), 40.62 (N-CH_2), 110.73, 112.92, 113.42, 126.44, 130.47 (C_{arom}), 142.61 (CH_2-$\underline{C}$=N), 153.24 (C=O).

HRMS (ESI): m/z calcd. for $C_{17}H_{14}BrN_3O_2$ 372.0269; Found: 372.0835 $[M + H]^+$.

IR (KBr), ν, cm^{-1} = 2958 (NH), 1738 (C=O), 1615 (C=N).

6-bromo-3-(2-(5-fluoro-1H-benzo[d]imidazol-2-yl)ethyl)benzo[d]oxazol-2(3H)-one (**4c**)

Brown solid, yield 2.12 g (94%), m.p. 217–219 °C.

^{1}H NMR (400 MHz, DMSO-d_6), δ: 2.71, 3.22 (2t, J = 6.9 Hz, 1.6H + 0.4H, CH_2), 4.01, 4.25 (2t, J = 6.9 Hz, 1.6H + 0.4H), 6.93–6.99 (m, 0.4H, H_{arom}), 7.18 (d, J = 8.3 Hz, 0.4H, H_{arom}), 7.24–7.37 (m, 2.2H, H_{arom}), 7.41 (d, J = 8.4 Hz, 2H, H_{arom}), 7.63 (s, 1H, H_{arom}), 12.45 (s, 1H, NH).

^{13}C NMR (101 MHz, DMSO-d_6), δ: 28.31 ($\underline{C}H_2$-C), 41.10 (N-CH_2), 106.11, 109.28, 110.86, 115.83, 115.86, 122.01, 136.63, 145.43, 154.76, 157.08 (C_{arom}), 159.40 (CH_2-$\underline{C}$=N), 173.44 (C=O).

Calcd for $C_{16}H_{11}BrFN_3O_2$, %: C, 51.09; H, 2.95; N, 11.17. Found, %: C 50.87; H 2.71; N 10.85.

IR (KBr), ν, cm^{-1} = 2931 (NH), 1717 (C=O).

6-bromo-3-(2-(5-chloro-1H-benzo[d]imidazol-2-yl)ethyl)benzo[d]oxazol-2(3H)-one (**4d**)

Brown solid, yield 2.12 g (90%), m.p. 180–182 °C.

^{1}H NMR (400 MHz, DMSO-d_6), δ: 3.09 (t, J = 7.0 Hz, 2H, CH_2), 3.51 (t, J = 7.1 Hz, 2H, CH_2), 6.53 (d, J = 8.2 Hz, 1H, H_{arom}), 6.75–6.83 (m, 2H, H_{arom}), 7.15 (d, J = 8.5 Hz, 1H, H_{arom}), 7.49 (d, J = 8.5 Hz, 1H, H_{arom}), 7.55 (s, 1H, H_{arom}), 9.80 (s, 1H, NH).

^{13}C NMR (101 MHz, DMSO-d_6), δ: 28.27 ($\underline{C}H_2$-C), 41.04 (N-CH_2), 106.12, 110.86, 115.86, 121.52, 121.98, 125.71, 136.60, 145.44 (C_{arom}), 154.87 (CH_2-$\underline{C}$=N), 173.43 (C=O).

Calcd for $C_{16}H_{11}BrClN_3O_2$, %: C, 48.94; H, 2.82; N, 10.70. Found, %: C 48.69; H 2.57; N 10.52.

IR (KBr), ν, cm^{-1} = 3111 (NH), 1727 (C=O).

Methyl 3-(6-bromo-2-oxobenzo[d]oxazol-3(2H)-yl)propanoate (**5**)

A mixture of carboxylic acid **2** (11.44 g, 40 mmol), methanol (200 mL), and a catalytic amount of sulfuric acid (a few drops) was heated at reflux for 24 h, then evaporated at reduced pressure. The residue was poured with aqueous 5% sodium carbonate solution to a pH of 8 and stirred for 5 min. The formed precipitate was filtered off, washed with water, and dried. The ester **5** was recrystallized from methanol.

Bright light brown solid, yield 11.27 g (94%), m.p. 97–99 °C.

^{1}H NMR (400 MHz, DMSO-d_6), δ: 2.79 (t, J = 6.8 Hz, 2H, CH_2), 3.56 (s, 3H, CH_3), 4.04 (t, J = 6.8 Hz, 2H, CH_2), 7.31 (d, J = 8.4 Hz, 1H, H_{arom}), 7.38–7.45 (m, 1H, H_{arom}), 7.64 (s, 1H, H_{arom}).

^{13}C NMR (101 MHz, DMSO-d_6), δ: 31.35 ($\underline{C}H_2$-CO), 37.93 (N-CH_2), 51.63 (CH_3), 111.09, 112.91, 113.48, 126.55, 130.43, 142.60 (C_{arom}), 153.21 (C=O), 171.04 ($\underline{C}OOCH_3$).

HRMS (ESI): m/z calcd. for $C_{11}H_{10}BrNO_4$ 300.9793; Found: 300.0303 $[M + H]^+$.

IR (KBr), ν, cm^{-1} = 1773, 1726 (2x C=O).

3-(6-bromo-2-oxobenzo[d]oxazol-3(2H)-yl)propanehydrazide (**6**)

Ester **5** (5.64 g, 19.8 mmol) was dissolved in propan-2-ol (50 mL), then hydrazine monohydrate (3 g, 60 mmol, dropwise) was added, and the mixture was refluxed for 24 h. The mixture was filtered, and the formed precipitate was filtered and washed with propan-2-ol and hexane. The crystals were recrystallised from a propan-2-ol (40 mL) and water (2 mL) mixture.

White solid, yield 4.96 g (83%), m.p. 168–170 °C.

^{1}H NMR (400 MHz, DMSO-d_6), δ: 2.50 (overlaps with DMSO-d_6, 2H, CH_2), 4.02 (t, J = 6.7 Hz, 2H, CH_2), 4.17 (s, 2H, NH_2), 7.23 (d, J = 8.3 Hz, 1H, H_{arom}), 7.43 (d, J = 8.4 Hz, 1H, H_{arom}), 7.64 (s, 1H, H_{arom}), 9.11 (s, 1H, NH).

^{13}C NMR (101 MHz, DMSO-d_6), δ: 31.76 ($\underline{C}H_2$-CO), 39.00 (N-CH_2), 111.29, 113.06, 113.61, 126.77, 130.77, 142.76 (C_{arom}), 153.43, 169.03 (2x C=O).

HRMS (ESI): m/z calcd. for $C_{10}H_{10}BrN_3O_3$ 300.9906; Found: 300.0434 $[M + H]^+$.

IR (KBr), ν, cm^{-1} = 3315, 3066 (NH_2, NH), 1747, 1632 (2x C=O).

3-(6-bromo-2-oxobenzo[d]oxazol-3(2H)-yl)-N-hydroxypropanamide (**7**)

The mixture of ester (0.30 g, 1 mmol) and $NH_2OH{\cdot}HCl$ (0.20 g, 3 mmol) in water/methanol (1:1, 6 mL) at 0–5 °C, a solution of KOH (0.39 g, 7 mmol) in water (1 mL) was added dropwise under stirring. The reaction mixture was stirred at this temperature for 24 h, then acidified with conc. HCl to pH 5–6. The mixture with the forming precipitate was left in the fridge for the night. The resultant precipitate was collected by filtration and washed with water. The compound was recrystallized from propan-2-ol.

Light brown solid, yield 0.23 g (77%), m.p. 169–171 °C.

^{1}H NMR (400 MHz, DMSO-d_6), δ: 2.43 (overlaps with DMSO-d_6, 2H, CH_2), 4.00 (t, J = 6.7 Hz, 1H, CH_2), 7.23 (d, J = 8.3 Hz, 1H, H_{arom}), 7.41 (d, J = 8.5 Hz, 1H, H_{arom}), 7.64 (s, 2H, H_{arom}), 8.79 (s, 1H, NH), 10.48 (s, 1H, OH).

^{13}C NMR (101 MHz, DMSO-d_6), δ: 30.39 ($\underline{C}H_2$-C), 38.61 (N-CH_2), 111.18, 112.84, 113.41, 126.56, 130.55, 142.57 (C_{arom}), 153.20 (C=O), 166.26 (O=C-NH).

HRMS (ESI): m/z calcd. for $C_{10}H_9BrN_2O_4$ 323.0960; Found: 323.0076 $[M + Na]^+$.

IR (KBr), ν, cm^{-1} = 3278 (OH), 2777 (NH), 1748, 1666 (2x C=O).

General Procedure for Preparation of Hydrazones (**8**–**13**)

To a hot solution of hydrazide **6** (0.30 g, 1 mmol) in propan-2-ol (15 mL), the corresponding aromatic or heterocyclic aldehyde (1,3 mmol) was added, and the mixture was heated at reflux for 3 h and then cooled down. The precipitate was filtered off, washed with propan-2-ol, and dried. The obtained solid was recrystallized from the mixture of propan-2-ol (40 mL) and 1,4-dioxane (5 mL).

N′-benzylidene-3-(6-bromo-2-oxobenzo[d]oxazol-3(2H)-yl)propanehydrazide (**8a**)

White solid, yield 0.31 g (80%), m.p. 211–213 °C.

^{1}H NMR (400 MHz, DMSO-d_6), δ: Z/E 70/30 2.71 (t, J = 6.7 Hz, 0.6H, CH_2), 3.09 (t, J = 6.8 Hz, 1.4H, CH_2), 4.06–4.17 (m, 2H, CH_2), 7.26–7.45 (m, 5H, H_{arom}), 7.48–7.57 (m, 2H, H_{arom}), 7.60–7.69 (m, 1H, H_{arom}), 7.93 (s, 0.7H, CH=N), 8.09 (s, 0.3H, CH=N), 11.41 (s, 0.7H, NH), 11.48 (s, 0.3H, NH).

^{13}C NMR (101 MHz, DMSO-d_6), δ: 30.27, 32.14 ($\underline{C}H_2$-C), 38.20, 38.40 (N-CH_2), 111.03, 111.19, 112.83, 112.86, 113.41, 113.44, 126.51, 126.67, 127.04, 128.71, 128.77, 129.77, 130.02, 130.59, 133.97, 134.13, 142.60, 143.32, 146.42, 153.24 (C_{arom}), 166.00, 171.85 (2x C=O).

HRMS (ESI): m/z calcd. for $C_{17}H_{14}BrN_3O_3$ 388.0219; Found: 388.0791 $[M + H]^+$.

IR (KBr), ν, cm^{-1} = 2958 (NH), 1781, 1667 (2x C=O), 1610 (C=N).

3-(6-bromo-2-oxobenzo[d]oxazol-3(2H)-yl)-N′-(4-methylbenzylidene)propanehydrazide (**8b**)

Brown solid, yield 0.16 g (41%), m.p. 152–154 °C.

^{1}H NMR (400 MHz, DMSO-d_6), δ: Z/E 67/33 2.31 (s, 3H, CH_3), 2.69 (t, J = 6.8 Hz, 0.67H, CH_2), 3.07 (t, J = 6.8 Hz, 1.33H, CH_2), 3.99 (t, J = 6.9 Hz, 0.33H, CH_2), 4.05–4.16 (m, 1.67H, CH_2), 7.15–7.36 (m, 3H, H_{arom}), 7.37–7.47 (m, 2H, H_{arom}), 7.51–7.57 (m, 1.33H, H_{arom}), 7.60–7.67 (m, 0.67H, H_{arom}), 7.89 (s, 0.67H, CH=N), 8.05 (s, 0.33H, CH=N), 11.41 (s, 1H, NH).

^{13}C NMR (101 MHz, DMSO-d_6), δ: 21.03 (CH_3), 30.27 ($\underline{C}H_2$-C), 38.24 (N-CH_2), 111.04, 112.84, 113.47, 126.63, 127.03, 129.33, 130.60, 131.28, 139.52, 142.60, 143.42, 146.50, 153.26 (C_{arom}), 165.90, 171.75 (2x C=O).

HRMS (ESI): m/z calcd. for $C_{18}H_{16}BrN_3O_3$ 402.0375; Found: 402.0897 $[M + H]^+$.

IR (KBr), ν, cm^{-1} = 3028 (NH), 1763, 1654 (2x C=O), 1602 (C=N).

3-(6-bromo-2-oxobenzo[d]oxazol-3(2H)-yl)-N′-(4-hydroxybenzylidene)propanehydrazide (**8c**)

White solid, yield 0.29 g (71%), m.p. 205–207 °C.

^{1}H NMR (400 MHz, DMSO-d_6), δ: Z/E 67/33 2.66 (t, J = 6.6 Hz, 0.66 H, CH_2), 3.04 (t, J = 6.7 Hz, 1.34H, CH_2), 4.05–4.15 (m, 2H, CH_2), 6.73–6.82 (m, 2H, H_{arom}), 7.26–7.51 (m, 4H, H_{arom}), 7.58 (s, 0.67H, H_{arom}), 7.64 (s, 0.33H, H_{arom}), 7.81 (s, 0.67H, CH=N), 7.96 (s, 0.33H, CH=N), 9.86 (s, 0.67H, OH), 9.90 (s, 0.33H, OH), 11.20 (s, 0.67H, NH), 11.26 (s, 0.33H, NH).

^{13}C NMR (101 MHz, DMSO-d_6), δ: 30.27, 32.14 (C$\underline{H}_2$-C), 38.22, 38.50 (N-CH_2), 111.06, 112.86, 113.43, 115.60, 125.02, 126.52, 128.41, 130.60, 130.62, 142.62, 143.65, 146.74, 153.27, 159.15 (C_{arom}), 165.58, 171.45 (2x C=O).

HRMS (ESI): *m*/*z* calcd. for $C_{17}H_{14}BrN_3O_4$ 404.0168; Found: 404.0695 $[M + H]^+$.

IR (KBr), ν, cm^{-1} = 3381 (OH) 2967 (NH), 1750, 1670 (2x C=O), 1615 (C=N).

3-(6-bromo-2-oxobenzo[d]oxazol-3(2H)-yl)-N′-(4-fluorobenzylidene)propanehydrazide (**8d**)

White solid, yield 0.35 g (85%), m.p. 218–220 °C.

^{1}H NMR (400 MHz, DMSO-d_6), δ: *Z*/*E* 68/32 2.70 (t, *J* = 6.7 Hz, 0.64H, CH_2), 3.08 (t, *J* = 6.7 Hz, 1.36H, CH_2), 4.05–4.16 (m, 2H, CH_2), 7.16–7.37 (m, 3H, H_{arom}), 7.39–7.46 (m, 1H, H_{arom}), 7.52–7.60 (m, 2H, H_{arom}), 7.64 (d, *J* = 2.3 Hz, 0.32H, H_{arom}), 7.71 (m, 0.68H, H_{arom}), 7.91 (s, 0.68H, CH=N), 8.08 (s, 0.32H, CH=N), 11.41 (s, 0.68H, H_{arom}), 11.48 (s, 0.32H, H_{arom}).

^{13}C NMR (101 MHz, DMSO-d_6), δ: 30.26, 32.13 (C$\underline{H}_2$-C), 38.23, 38.40 (N-CH_2), 111.03, 112.82, 113.45, 115.79 (dd, *J* = 21.9, 8.7 Hz), 126.53, 129.01 (dd, *J* = 41.1, 8.5 Hz), 130.58, 142.15, 145.31, 153.25, 162.88 (d, *J* = 247.3 Hz), 164.11 (C_{arom}), 166.02, 171.87 (2x C=O).

HRMS (ESI): *m*/*z* calcd. for $C_{17}H_{13}BrFN_3O_3$ 406.0124; Found: 406.0655 $[M + H]^+$.

IR (KBr), ν, cm^{-1} = 2960 (NH), 1759, 1665 (2x C=O), 1613 (C=N).

3-(6-bromo-2-oxobenzo[d]oxazol-3(2H)-yl)-N′-(4-chlorobenzylidene)propanehydrazide (**8e**)

White solid, yield 0.39 g (92%), m.p. 188–190 °C.

^{1}H NMR (400 MHz, DMSO-d_6), δ: *Z*/*E* 70/30 2.71 (t, *J* = 6.7 Hz, 0.6H, CH_2), 3.08 (t, *J* = 6.7 Hz, 1,4H, CH_2), 4.05–4.16 (m, 2H, CH_2), 7.29 (d, *J* = 8.4 Hz, 0.3H, H_{arom}), 7.34 (d, *J* = 8.3 Hz, 0.7H, H_{arom}), 7.42 (d, *J* = 8.6 Hz, 2H + 0.3H, H_{arom}), 7.48 (d, *J* = 8.6 Hz, 0.7H, H_{arom}), 7.53 (d, *J* = 8.7 Hz, 2H, H_{arom}), 7.58–7.71 (m, 1H, H_{arom}), 7.90 (s, 0.7H, CH=N), 8.07 (s, 0.3H, CH=N), 11.46 (s, 0.7H, NH), 11.54 (s, 0.3H, NH).

^{13}C NMR (101 MHz, DMSO-d_6), δ: 30.25, 32.14 (C$\underline{H}_2$-C), 38.23, 38.39 (N-CH_2), 111.05, 111.20, 112.83, 112.88, 113.43, 113.49, 126.55, 128.28, 128.69, 128.79, 128.88, 130.58, 132.91, 133.11, 134.20, 134.47, 142.02, 142.59, 145.13, 153.25 (C_{arom}), 166.13, 171.97 (2x C=O).

HRMS (ESI): *m*/*z* calcd. for $C_{17}H_{13}BrClN_3O_3$ 422.9829; Found: 422.0393 $[M + H]^+$.

IR (KBr), ν, cm^{-1} = 2975 (NH), 1776, 1676 (2x C=O), 1609 (C=N).

3-(6-bromo-2-oxobenzo[d]oxazol-3(2H)-yl)-N′-(3-nitrobenzylidene)propanehydrazide (**8f**)

White solid, yield 0.32 g (74%), m.p. 219–221 °C.

^{1}H NMR (400 MHz, DMSO-d_6), δ: *Z*/*E* 66/34 2.74 (t, *J* = 6.7 Hz, 0.68H, CH_2), 3.12 (t, *J* = 6.7 Hz, 1.32H, CH_2), 4.07–4.17 (m, 2H, CH_2), 7.26–7.45 (m, 2H, H_{arom}), 7.50 (s, 0.66H, H_{arom}), 7.65 (s, 1.34H, H_{arom}), 7.96 (d, *J* = 7.8 Hz, 0.66H, H_{arom}), 8.03 (s, 0.66H, H_{arom}), 8.08 (d, *J* = 7.6 Hz, 0.34H, H_{arom}), 8.17–8.25 (m, 1.34H, H_{arom}), 8.32 (s, 0.66H, CH=N), 8.47 (s, 0.34H, CH=N), 11.64 (s, 0.66H, NH), 11.73 (s, 0.34H, NH).

^{13}C NMR (101 MHz, DMSO-d_6), δ: 30.26, 32.14 (C$\underline{H}_2$-C), 38.23, 38.34 (N-CH_2), 111.0, 111.20, 112.75, 112.87, 113.42, 120.85, 121.04, 124.02, 124.23, 126.52, 130.27, 130.39, 130.58, 132.70, 135.80, 136.06, 141.09, 142.53, 142.60, 144.03, 148.13, 148.16, 153.25 (C_{arom}), 166.46, 172.18 (2x C=O).

HRMS (ESI): *m*/*z* calcd. for $C_{17}H_{13}BrN_4O_5$ 433.0069; Found: 433.0633 $[M + H]^+$.

IR (KBr), ν, cm^{-1} = 3016 (NH), 1762, 1659 (2x C=O), 1613 (C=N).

3-(6-bromo-2-oxobenzo[d]oxazol-3(2H)-yl)-N′-(4-nitrobenzylidene)propanehydrazide (**8g**)

Pale-yellow solid, yield 0.37 g (85%), m.p. 204–206 °C.

^{1}H NMR (400 MHz, DMSO-d_6), δ: *Z*/*E* 70/30 2.75 (t, *J* = 6.6 Hz, 0.6H, CH_2), 3.12 (t, *J* = 6.7 Hz, 1.4H, CH_2), 4.07–4.18 (m, 2H, CH_2), 7.29 (d, *J* = 8.4 Hz, 0.3H, H_{arom}), 7.35 (d, *J* = 8.3 Hz, 0.7H, H_{arom}), 7.38–7.46 (m, 1H, H_{arom}), 7.51 (s, 0.7H, H_{arom}), 7.62 (s, 0.3H, H_{arom}), 7.74 (d, *J* = 8.3 Hz, 1.3H, H_{arom}), 7.91 (d, *J* = 8.4 Hz, 0.6H, H_{arom}), 8.00 (s, 0.7H, H_{arom}), 8.19 (d, *J* = 7.8 Hz, 1.40H + 0.3H, H_{arom} + CH=N), 8.25 (d, *J* = 8.4 Hz, 0.7H, CH=N), 11.71 (s, 0.7H, NH), 11.78 (s, 0.3H, NH).

^{13}C NMR (101 MHz, DMSO-d_6), δ: 30.27, 32.17 ($\underline{C}H_2$-C), 38.20, 38.29 (N-CH_2), 111.06, 112.79, 113.51, 123.89, 126.57, 127.52, 130.55, 140.91, 142.54, 143.94, 147.56, 153.23 (C_{arom}), 166.53, 172.34 (2x C=O).

HRMS (ESI): *m*/*z* calcd. for $C_{17}H_{13}BrN_4O_5$ 433.0069; Found: 433.0613 $[M + H]^+$.

IR (KBr), ν, cm^{-1} = 2955 (NH), 1781, 1671 (2x C=O), 1609 (C=N).

3-(6-bromo-2-oxobenzo[d]oxazol-3(2H)-yl)-N′-(2,4-dimethylbenzylidene)propanehydrazide (**8h**)

White solid, yield 0.43 g (97%), m.p. 201–203 °C.

^{1}H NMR (400 MHz, DMSO-d_6), δ: *Z*/*E* 67/33 2.64 (t, *J* = 6.7 Hz, 0.66H, CH_2), 3.04 (t, *J* = 6.7 Hz, 1.34H, CH_2), 3.77–3.84 (m, 6H, 2x OCH_3), 4.05–4.14 (m, 2H, CH_2), 6.50 (d, *J* = 8.7 Hz, 0.67H, H_{arom}), 6.56–6.61 (m, 1.33H, H_{arom}), 7.28 (d, *J* = 8.4 Hz, 0.33H, H_{arom}), 7.32 (d, *J* = 8.3 Hz, 0.67H, H_{arom}), 7.40–7.47 (m, 1H + 0.67H, H_{arom}), 7.56 (d, *J* = 1.8 Hz, 0.67H, H_{arom}), 7.64 (d, *J* = 2.3 Hz, 0.33H, H_{arom}), 7.68 (d, *J* = 8.5 Hz, 0.33H, H_{arom}), 8.15 (s, 0.67H, CH=N), 8.32 (s, 0.33H, CH=N), 11.21 (s, 0.67H, NH), 11.32 (s, 0.33H, NH).

^{13}C NMR (101 MHz, DMSO-d_6), δ: 30.33, 32.18 ($\underline{C}H_2$-C), 38.30, 38.51 (N-CH_2), 55.41, 55.45, 55.73, 55.78 (2x OCH_3), 98.10, 98.26, 106.33, 111.02, 111.20, 112.86, 113.46, 114.83, 126.24, 126.52, 126.61, 130.61, 139.10, 142.02, 142.61, 153.25, 158.87, 159.06, 162.14, 162.42 (C_{arom}), 165.47, 171.47 (2x C=O).

HRMS (ESI): *m*/*z* calcd. for $C_{19}H_{18}BrN_3O_5$ 448.0430; Found: 448.1001 $[M + H]^+$.

IR (KBr), ν, cm^{-1} = 2964 (NH), 1792, 1662 (2x C=O), 1615 (C=N).

3-(6-bromo-2-oxobenzo[d]oxazol-3(2H)-yl)-N′-(3,4-dimethylbenzylidene)propanehydrazide (**8i**)

White solid, yield 0.31 g (70%), m.p. 191–193 °C.

^{1}H NMR (400 MHz, DMSO-d_6), δ: *Z*/*E* 64/36 2.69 (t, *J* = 6.7 Hz, 0.72H, CH_2), 3.07 (t, *J* = 6.7 Hz, 1.28H, CH_2), 3.78 (s, 6H, 2x OCH_3), 4.01–4.17 (m, 2H, CH_2), 6.90–7.05 (m, 2H, H_{arom}), 7.13 (d, *J* = 8.3 Hz, 0.36H, H_{arom}), 7.20 (s, 0.64H, H_{arom}), 7.24 (s, 0.36H, H_{arom}), 7.29 (d, *J* = 8.4 Hz, 0.64H, H_{arom}), 7.37–7.45 (m, 1H, H_{arom}), 7.54 (s, 0.64H, H_{arom}), 7.63 (s, 0.36H, H_{arom}), 7.81 (s, 0.64H, CH=N), 7.99 (s, 0.36H, CH=N), 11.27 (s, 0.64H, NH), 11.35 (s, 0.36H, NH).

^{13}C NMR (101 MHz, DMSO-d_6), δ: 30.32, 32.12 ($\underline{C}H_2$-C), 38.43, 38.48 (N-CH_2), 55.43, 55.55 (2x OCH_3), 108.20, 108.62, 110.96, 111.23, 111.41, 111.43, 112.82, 112.88, 113.40, 113.43, 120.87, 121.80, 126.50, 126.54, 126.71, 126.80, 130.60, 142.58, 142.61, 143.56, 146.67, 148.94, 149.01, 150.45, 150.70, 153.28 (C_{arom}), 165.74, 171.66 (2x C=O).

HRMS (ESI): *m*/*z* calcd. for $C_{19}H_{18}BrN_3O_5$ 448.0430; Found: 448.1005 $[M + H]^+$.

IR (KBr), ν, cm^{-1} = 2960 (NH), 1791, 1667 (2x C=O), 1614 (C=N).

3-(6-bromo-2-oxobenzo[d]oxazol-3(2H)-yl)-N′-(2,3,4-trimethylbenzylidene)propanehydrazide (**8j**)

White solid, yield 0.24 g (50%), m.p. 216–218 °C.

^{1}H NMR (400 MHz, DMSO-d_6), δ: *Z*/*E* 66/34 2.66 (t, *J* = 6.7 Hz, 0.68H, CH_2), 3.05 (t, *J* = 6.7 Hz, 1.32H, CH_2), 3.72–3.86 (m, 9H, 3CH_3), 4.04–4.16 (m, 2H, CH_2), 6.79 (d, *J* = 8.8 Hz, 0.66H, H_{arom}), 6.89 (d, *J* = 8.9 Hz, 0.34H, H_{arom}), 7.21–7.35 (m, 1.66H, H_{arom}), 7.42 (d, *J* = 8.2 Hz, 1H, H_{arom}), 7.51 (d, *J* = 8.9 Hz, 0.34H, H_{arom}), 7.54 (s, 0.66H, H_{arom}), 7.64 (s, 0.34H, H_{arom}), 8.09 (s, 0.66H, CH=N), 8.23 (s, 0.34H, CH=N), 11.26 (s, 0.66H, NH), 11.40 (s, 0.34H, NH).

^{13}C NMR (101 MHz, DMSO-d_6), δ: 30.33, 32.19 ($\underline{C}H_2$-C), 38.34 (N-CH_2), 55.97, 60.49, 61.74 (3OCH_3), 108.52, 111.02, 113.47, 120.16, 126.54, 130.60, 139.20, 141.47, 142.59, 152.37, 153.26, 154.87 (C_{arom}), 165.65, 171.58 (2x C=O).

HRMS (ESI): *m*/*z* calcd. for $C_{20}H_{20}BrN_3O_6$ 478.0535; Found: 478.1119 $[M + H]^+$.

IR (KBr), ν, cm^{-1} = 2999 (NH), 1761 (2x C=O), 1639 (C=N).

N′-(3,5-bis(trifluoromethyl)benzylidene)-3-(6-bromo-2-oxobenzo[d]oxazol-3(2H)-yl)propanehydrazide (**8k**)

White solid, yield 0.51 g (97%), m.p. 221–223 °C.

^{1}H NMR (400 MHz, DMSO), δ: *Z*/*E* 63/37 2.76 (t, *J* = 6.6 Hz, 0.74H, CH_2), 3.14 (t, *J* = 6.6 Hz, 1.26H, CH_2), 4.07–4.17 (m, 2H, CH_2), 7.26–7.37 (m, 1.63H, H_{arom}), 7.41 (d, *J* = 8.4 Hz, 0.37H, H_{arom}), 7.49 (s, 0.63H, H_{arom}), 7.62 (s, 0.37H, H_{arom}), 8.03–8.12 (m, 1.74H, H_{arom}), 8.24 (s, 1.26H + 0.37H, H_{arom} + CH=N), 8.30 (s, 0.63H, CH=N), 11.75 (s, 0.63H, NH), 11.86 (s, 0.37H, NH).

^{13}C NMR (101 MHz, DMSO-d_6), δ: 30.21, 32.11 ($\underline{C}H_2$-C), 38.30 (N-CH_2), 110.95, 111.21, 112.72, 112.86, 113.34, 113.42, 119.09, 121.81, 122.62, 122.89, 124.52, 126.45, 126.53, 126.90, 127.10, 127.24, 130.24, 130.58, 130.90, 131.06 (d, *J* = 33.0 Hz), 136.83, 137.11, 140.27, 142.50, 142.62, 143.06, 153.25 (C_{arom}), 166.69, 172.38 (2X C=O).

HRMS (ESI): *m*/*z* calcd. for $C_{19}H_{12}BrF_6N_3O_3$ 524.9966; Found: 524.0537 $[M + H]^+$.

IR (KBr), ν, cm^{-1} = 3026 (NH), 1760, 1655 (2x C=O), 1627 (C=N).

3-(6-bromo-2-oxobenzo[d]oxazol-3(2H)-yl)-N′-(4-(dimethylamino)benzylidene)propanehydrazide (**8l**)

White solid, yield 0.24 g (56%), m.p. 254–256 °C.

^{1}H NMR (400 MHz, DMSO-d_6), δ: *Z*/*E* 66/34 2.65 (t, *J* = 6.6 Hz, 0.68H, CH_2), 2.95 (s, 6H, 2x CH_3), 3.01–3.07 (m, 1.32H, CH_2), 4.03–4.14 (m, 2H, CH_2), 6.65 (d, 1.32H, H_{arom}), 6.71 (d, *J* = 8.4 Hz, 0.68H, H_{arom}), 7.28 (d, *J* = 8.4 Hz, 1.66H, H_{arom}), 7.33 (d, *J* = 1.5 Hz, 0.68H, H_{arom}), 7.38–7.48 (m, 1.66H, H_{arom}), 7.56 (s, 0.66H, H_{arom}), 7.63 (s, 0.34H, H_{arom}), 7.77 (s, 0.66H, CH=N), 7.92 (s, 0.34H, CH=N), 11.10 (s, 0.66H, NH), 11.17 (s, 0.34H, NH).

^{13}C NMR (101 MHz, DMSO-d_6), δ: 30.30, 32.15 ($\underline{C}H_2$-C), 38.36 (N-CH_2), 38.55, 39.78 (2x CH_3), 111.01, 111.22, 111.69, 111.74, 112.87, 113.45, 121.35, 126.52, 127.93, 128.38, 130.63, 142.63, 144.18, 147.27, 151.24, 151.48, 153.27 (C_{arom}), 165.31, 171.24 (2x C=O).

HRMS (ESI): *m*/*z* calcd. for $C_{19}H_{19}BrN_4O_3$ 431.0641; Found: 431.122 $[M + H]^+$.

IR (KBr), ν, cm^{-1} = 2902 (NH), 1765, 1662 (2x C=O), 1607 (C=N).

3-(6-bromo-2-oxobenzo[d]oxazol-3(2H)-yl)-N′-(4-(diethylamino)benzylidene)propanehydrazide (**8m**)

Pale-yellow solid, yield 0.40 g (88%), m.p. 216–218 °C.

^{1}H NMR (400 MHz, DMSO-d_6), δ: *Z*/*E* 66/34 1.09 (t, *J* = 7.0 Hz, 6H, 2x CH_3), 2.65 (t, *J* = 6.8 Hz, 0.68H, CH_2), 3.02 (t, *J* = 6.7 Hz, 1.32H, CH_2), 3.31–3.39 (m, 4H, 2x $C\underline{H}_2CH_3$), 4.03–4.16 (m, 2H, CH_2), 6.60 (d, *J* = 8.4 Hz, 1.32H, H_{arom}), 6.66 (d, *J* = 8.4 Hz, 0.68H, H_{arom}), 7.22–7.37 (m, 2.34H, H_{arom}), 7.43 (t, *J* = 8.4 Hz, 1.66H, H_{arom}), 7.58 (s, 0.66H, H_{arom}), 7.64 (s, 0.34H, H_{arom}), 7.75 (s, 0.66H, CH=N), 7.90 (s, 0.34H, CH=N), 11.07 (s, 0.66H, NH), 11.12 (s, 0.34H, NH).

^{13}C NMR (101 MHz, DMSO-d_6), δ: 12.44 (2x CH_3), 30.30, 32.14 ($\underline{C}H_2$-C), 38.33 (N-CH_2), 43.71 (2x $\underline{C}H_2CH_3$), 110.95, 111.21, 112.89, 113.41, 120.41, 126.52, 128.28, 128.72, 130.63, 142.63, 144.23, 147.31, 148.57, 153.24 (C_{arom}), 165.20, 171.14 (2x C=O).

HRMS (ESI): *m*/*z* calcd. for $C_{21}H_{23}BrN_4O_3$ 459.0954; Found: 459.1472 $[M + H]^+$.

IR (KBr), ν, cm^{-1} = 2969 (NH), 1739, 1673 (2x C=O).

3-(6-bromo-2-oxobenzo[d]oxazol-3(2H)-yl)-N′-((5-nitrofuran-2-yl)methylene)propanehydrazide (**9a**)

Yellow solid, yield 0.40 g (95%), m.p. 213–215 °C.

^{1}H NMR (400 MHz, DMSO-d_6), δ: *Z*/*E* 64/36 2.75 (t, *J* = 6.7 Hz, 0.72H, CH_2), 3.07 (t, *J* = 6.8 Hz, 1.28H, CH_2), 4.07–4.15 (m, 2H, CH_2), 7.14 (d, *J* = 3.9 Hz, 0.64H, H_{arom}), 7.19 (d, *J* = 4.0 Hz, 0.36H, H_{arom}), 7.29 (d, *J* = 8.4 Hz, 0.36H, H_{arom}), 7.34 (d, *J* = 8.3 Hz, 0.64H, H_{arom}), 7.38–7.45 (m, 1H, H_{arom}), 7.58 (s, 0.64H, H_{arom}), 7.63 (s, 0.36H, H_{arom}), 7.75 (d, *J* = 3.9 Hz, 1H, H_{arom}), 7.88 (s, 0.64H, CH=N), 8.05 (s, 0.36H, CH=N), 11.81 (s, 0.64H, NH), 11.86 (s, 0.36H, NH).

^{13}C NMR (101 MHz, DMSO-d_6), δ: 30.23, 32.22 ($\underline{C}H_2$-C), 37.95, 38.23 (N-CH_2), 111.10, 111.18, 112.79, 112.89, 113.39, 113.45, 114.60, 114.69, 114.80, 115.41, 126.57, 130.54, 131.47, 134.39, 142.58, 142.61, 151.44, 153.26 (C_{arom}), 166.73, 172.22 (2x C=O).

HRMS (ESI): *m*/*z* calcd. for $C_{15}H_{11}BrN_4O_6$ 423.9862; Found: 423.0412 $[M + H]^+$.

IR (KBr), ν, cm^{-1} = 3034 (NH), 1764, 1667 (2x C=O), 1611 (C=N).

3-(6-bromo-2-oxobenzo[d]oxazol-3(2H)-yl)-N′-(thiophen-2-ylmethylene)propanehydrazide (**9b**)

White solid, yield 0.39 g (99%), m.p. 205–207 °C.

^{1}H NMR (400 MHz, DMSO-d_6), δ: *Z*/*E* 58/42 2.68 (t, *J* = 6.7 Hz, 0.84H, CH_2), 3.01 (t, *J* = 6.8 Hz, 1.16H, CH_2), 4.04–4.14 (m, 2H, CH_2), 7.05–7.14 (m, 1H, H_{arom}), 7.25–7.46 (m, 3H, H_{arom}), 7.56–7.66 (m, 2H, H_{arom}), 8.12 (s, 0.58H, CH=N), 8.30 (s, 0.42H, CH=N), 11.38 (s, 0.58H, NH), 11.42 (s, 0.42H, NH).

^{13}C NMR (101 MHz, DMSO-d_6), δ: 30.11, 32.11 ($\underline{C}H_2$-C), 38.04, 38.38 (N-CH_2), 111.06, 111.18, 112.85, 113.41, 126.51, 127.80, 127.84, 128.35, 128.86, 130.31, 130.58, 130.94, 138.51, 138.72, 138.88, 141.62, 142.59, 142.62, 153.23, 153.25 (C_{arom}), 165.84, 171.40 (2x C=O).

HRMS (ESI): *m*/*z* calcd. for $C_{15}H_{12}BrN_3O_3S$ 394.9783; Found: 394.0314 $[M + H]^+$.

IR (KBr), ν, cm^{-1} = 2890 (NH), 1767, 1661 (2x C=O), 1613 (C=N).

3-(6-bromo-2-oxobenzo[d]oxazol-3(2H)-yl)-N′-((5-nitrothiophen-2-yl)methylene)propanehydrazide (**9c**)

Yellow solid, yield 0.43 g (99%), m.p. 250–252 °C.

^{1}H NMR (400 MHz, DMSO-d_6), δ: *Z*/*E* 70/30 δ 2.74 (t, *J* = 6.6 Hz, 0.6H, CH_2), 3.04 (t, *J* = 6.6 Hz, 1.4H, CH_2), 4.05–4.15 (m, 2H, CH_2), 7.29 (d, *J* = 8.4 Hz, 0.3H, H_{arom}), 7.34 (d, *J* = 8.3 Hz, 0.7H, H_{arom}), 7.38–7.48 (m, 1.7H, H_{arom}), 7.52 (d, *J* = 4.5 Hz, 0.3H, H_{arom}), 7.56 (s, 0.7H, H_{arom}), 7.63 (s, 0.3H, H_{arom}), 8.06 (d, *J* = 4.3 Hz, 0.7H, H_{arom}), 8.09 (s, 0.7H + 0.3H, H_{arom} + CH=N), 8.35 (s, 0.3H, CH=N), 11.81, 11.84 (2s, 1H, NH).

^{13}C NMR (101 MHz, DMSO-d_6), δ: 30.07, 32.15 ($\underline{C}H_2$-C), 38.15 (N-CH_2), 111.04, 113.52, 126.54, 130.42, 136.62, 139.98, 142.60, 146.35, 150.43, 153.22 (C_{arom}), 166.62, 172.18 (2x C=O).

HRMS (ESI): *m*/*z* calcd. for $C_{15}H_{11}BrN_4O_5S$ 439.9634; Found: 439.0181 $[M + H]^+$.

IR (KBr), ν, cm^{-1} = 2990 (NH), 1781, 1655 (2x C=O), 1613 (C=N).

3-(6-bromo-2-oxobenzo[d]oxazol-3(2H)-yl)-N′-((5-bromothiophen-2-yl)methylene)propanehydrazide (**9d**)

Light brown solid, yield 0.42 g (89%), m.p. 216–218 °C.

^{1}H NMR (400 MHz, DMSO-d_6), δ: *Z*/*E* 60/40 2.68 (t, *J* = 6.6 Hz, 0.8H, CH_2), 2.98 (t, *J* = 6.7 Hz, 1.2H, CH_2), 4.00–4.13 (m, 2H, CH_2), 7.15–7.34 (m, 3H, H_{arom}), 7.41 (d, *J* = 8.8 Hz, 1H, H_{arom}), 7.60 (d, *J* = 16.0 Hz, 1H, H_{arom}), 8.01 (s, 0.6H, CH=N), 8.23 (s, 0.4H, CH=N), 11.45, 11.49 (2s, 1H, NH).

^{13}C NMR (101 MHz, DMSO-d_6), δ: 30.06, 32.11 ($\underline{C}H_2$-C), 38.11 (N-CH_2), 111.03, 112.84, 113.45, 114.14, 114.63, 126.50, 130.77, 137.58, 140.64, 142.62, 153.21 (C_{arom}), 166.00, 171.58 (2x C=O).

HRMS (ESI): *m*/*z* calcd. for $C_{15}H_{11}Br_2N_3O_3S$ 471.8888; Found: 471.9395 $[M + H]^+$.

IR (KBr), ν, cm^{-1} = 3115 (NH), 1760, 1668 (2x C=O), 1614 (C=N).

3-(6-bromo-2-oxobenzo[d]oxazol-3(2H)-yl)-N′-(pyridin-4-ylmethylene)propanehydrazide (**10**)

Light brown solid, yield 0.37 g (94%), m.p. 205–207 °C.

^{1}H NMR (400 MHz, DMSO-d_6), δ: *Z*/*E* 72/28 2.74 (t, *J* = 6.6 Hz, 0.56H, CH_2), 3.11 (t, *J* = 6.8 Hz, 1.44H, CH_2), 4.05–4.22 (m, 2H, CH_2), 7.29 (d, *J* = 8.4 Hz, 0.28H, H_{arom}), 7.35 (d, *J* = 8.3 Hz, 0.72H, H_{arom}), 7.39–7.50 (m, 2.44H, H_{arom}), 7.56 (s, 0.72H, H_{arom}), 7.59 (d, *J* = 5.1 Hz, 0.56H, H_{arom}), 7.64 (s, 0.28H, H_{arom}), 7.90 (s, 0.72H, H_{arom}), 8.08 (s, 0.28H, H_{arom}), 8.56 (d, *J* = 5.0 Hz, 1H + 0.44H, H_{arom} + CH=N), 8.61 (d, *J* = 5.0 Hz, 0.56H, CH=N), 11.68 (s, 0.72H, NH), 11.75 (s, 0.28H, NH).

^{13}C NMR (101 MHz, DMSO-d_6), δ: 30.24, 32.14 ($\underline{C}H_2$-C), 38.17, 38.27 (N-CH_2), 111.06, 111.19, 112.84, 112.88, 113.43, 113.48, 120.62, 120.97, 126.56, 130.57, 140.85, 141.09, 141.36, 142.59, 144.01, 150.12, 150.21, 153.24 (C_{arom}), 166.51, 172.34 (2x C=O).

HRMS (ESI): *m*/*z* calcd. for $C_{16}H_{13}BrN_4O_3$ 389.0171; Found: 389.0746 $[M + H]^+$.

IR (KBr), ν, cm^{-1} = 2957 (NH), 1771, 1674 (2x C=O), 1600 (C=N).

3-(6-bromo-2-oxobenzo[d]oxazol-3(2H)-yl)-N′-(naphthalen-1-ylmethylene)propanehydrazide (**11**)

Pale-yellow solid, yield 0.43 g (99%), m.p. 192–194 °C.

^{1}H NMR (400 MHz, DMSO-d_6), δ: *Z*/*E* 67/33 2.76 (t, *J* = 6.7 Hz, 0.67H, CH_2), 3.18 (t, *J* = 6.8 Hz, 1.33H, CH_2), 4.09–4.21 (m, 2H, CH_2), 7.29–7.47 (m, 2H, H_{arom}), 7.49–7.68 (m, 4H, H_{arom}), 7.77 (d, *J* = 7.2 Hz, 0.67H, H_{arom}), 7.83 (d, *J* = 7.2 Hz, 0.33H, H_{arom}), 7.99 (d, *J* = 7.8 Hz, 2H, H_{arom}), 8.45 (d, *J* = 8.0 Hz, 0.67H, H_{arom}), 8.67 (d, *J* = 12.8 Hz, 0.33 + 0.67H, H_{arom}+ CH=N), 8.78 (d, *J* = 8.5 Hz, 0.33H, CH=N), 11.47 (s, 0.67H, NH), 11.58 (s, 0.33H, NH).

^{13}C NMR (101 MHz, DMSO-d_6), δ: 30.34, 32.17 ($\underline{C}H_2$-C), 38.18, 38.44 (N-CH_2), 111.09, 111.20, 112.80, 112.88, 113.41, 123.29, 124.28, 125.50, 126.21, 126.28, 126.35, 126.48, 126.53, 127.24, 127.36, 128.12, 128.77, 128.84, 129.26, 129.36, 130.05, 130.08, 130.22, 130.55, 130.60, 133.44, 133.51, 142.58, 142.62, 142.65, 146.49, 153.27 (C_{arom}), 166.03, 171.79 (2x C=O).

HRMS (ESI): *m*/*z* calcd. for $C_{21}H_{16}BrN_3O_3$ 438.0375; Found: 438.0939 $[M + H]^+$.

IR (KBr), ν, cm^{-1} = 2964 (NH), 1788, 1667 (2x C=O), 1619 (C=N).

3-(6-bromo-2-oxobenzo[d]oxazol-3(2H)-yl)-N′-((2-hydroxynaphthalen-1-yl)methylene)propanehydrazide (**12**)

White solid, yield 0.45 g (99%), m.p. 260–262 °C.

^{1}H NMR (400 MHz, DMSO-d_6), δ: *Z*/*E* 70/30 2.77 (t, *J* = 6.6 Hz, 1.4H, CH_2), 3.15 (t, *J* = 6.7 Hz, 0.6H, CH_2), 4.10–4.19 (m, 2H, CH_2), 7.15–7.23 (m, 1H, H_{arom}), 7.35–7.44 (m, 3H, H_{arom}), 7.47–7.53 (m, 0.3H, H_{arom}), 7.54–7.61 (m, 1H, H_{arom}), 7.65 (s, 0.7H, H_{arom}), 7.81–7.93 (m, 2H, H_{arom}), 8.21 (d, *J* = 8.6 Hz, 0.7H, H_{arom}), 8.53 (d, *J* = 8.6 Hz, 0.3H, H_{arom}), 8.85 (s, 0.3H, CH=N), 9.07 (s, 0.7H, CH=N), 10.89 (s, 0.3H, OH), 11.42 (s, 0.3H, OH), 11.82 (s, 0.7H, NH), 12.43 (s, 0.7H, NH).

^{13}C NMR (101 MHz, DMSO-d_6), δ: 30.72, 31.93 ($\underline{C}H_2$-C), 38.36 (N-CH_2), 108.48, 109.96, 111.15, 111.22, 112.81, 112.91, 113.38, 113.46, 118.17, 118.78, 120.95, 122.80, 123.44, 123.55, 126.48, 126.56, 127.79, 127.82, 128.10, 128.77, 128.94, 130.59, 130.65, 131.48, 132.37, 132.72, 142.64, 145.50, 153.30, 156.77, 157.80 (C_{arom}), 165.69, 171.01 (2x C=O).

HRMS (ESI): *m*/*z* calcd. for $C_{21}H_{16}BrN_3O_4$ 454.0324; Found: 454.0842 $[M + H]^+$.

IR (KBr), ν, cm^{-1} = 3304 (OH), 3070 (NH), 1760, 1689 (2x C=O), 1622 (C=N).

3-(6-bromo-2-oxobenzo[d]oxazol-3(2H)-yl)-N′-(naphthalen-2-ylmethylene)propanehydrazide (**13**)

White solid, yield 0.32 g (72%), m.p. 214–216 °C.

^{1}H NMR (400 MHz, DMSO-d_6), δ: *Z*/*E* 68/32 2.74 (t, *J* = 6.7 Hz, 0.64H, CH_2), 3.14 (t, *J* = 6.7 Hz, 1.36H, CH_2), 4.08–4.22 (m, 2H, CH_2), 7.31 (d, *J* = 8.4 Hz, 0.32H, H_{arom}), 7.36 (d, *J* = 8.3 Hz, 0.68H, H_{arom}), 7.40–7.46 (m, 1H, H_{arom}), 7.50–7.59 (m, 2.68H, H_{arom}), 7.64 (s, 0.32H, H_{arom}), 7.74 (d, *J* = 8.6 Hz, 0.68H, H_{arom}), 7.83–8.03 (m, 4H, H_{arom}), 8.09 (s, 0.32H + 0.68H, H_{arom}+ CH=N), 8.24 (s, 0.32H, CH=N), 11.53 (s, 1H, NH).

^{13}C NMR (101 MHz, DMSO-d_6), δ: 30.32, 32.18 ($\underline{C}H_2$-C), 38.23, 38.43 (N-CH_2), 111.07, 111.22, 112.84, 112.87, 113.42, 113.48, 122.15, 122.65, 126.53, 126.73, 127.03, 127.11, 127.76, 128.26, 128.29, 128.36, 128.44, 128.51, 128.68, 130.62, 131.72, 131.90, 132.81, 133.56, 133.70, 142.61, 143.44, 146.39, 153.28 (C_{arom}), 166.05, 171.89 (2x C=O).

HRMS (ESI): *m*/*z* calcd. for $C_{21}H_{16}BrN_3O_3$ 438.0375; Found: 438.0947 $[M + H]^+$.

IR (KBr), ν, cm^{-1} = 3280 (NH), 1748, 1679 (2x C=O), 1609 (C=N).

6-bromo-3-(3-(3,5-dimethyl-1H-pyrazol-1-yl)-3-oxopropyl)benzo[d]oxazol-2(3H)-one (**14**)

To a solution of hydrazide **6** (0.40 g, 1.3 mmol) in propan-2-ol (25 mL), pentane-2,4-dione (0.20 g, 2 mmol) and hydrochloric acid (3 drops) were added, and the mixture was refluxed for 18 h. The formed precipitate was filtered off, washed with propan-2-ol, and dried. The obtained solid was recrystallized from propan-2-ol.

White solid, yield 0.26 g (56%), m.p. 150–152 °C.

^{1}H NMR (400 MHz, DMSO-d_6), δ: 2.10 (s, 3H, CH_3), 2.41 (s, 3H, CH_3), 3.49 (t, J = 6.7 Hz, 2H, CH_2), 4.16 (t, J = 6.7 Hz, 2H, CH_2), 6.14 (s, 1H, H_{arom}), 7.32 (d, J = 8.3 Hz, 1H, H_{arom}), 7.42 (d, J = 8.3 Hz, 1H, H_{arom}), 7.63 (s, 1H, H_{arom}).

^{13}C NMR (101 MHz, DMSO-d_6), δ: 13.38, 13.99 (2x CH_3), 32.93 ($\underline{C}H_2$-C), 37.73 (N-CH_2), 110.97, 111.27, 112.81, 113.39, 126.48, 130.56, 142.63, 143.28, 151.67 (C_{arom}), 153.24, 171.00 (2x C=O).

HRMS (ESI): m/z calcd. for $C_{15}H_{14}BrN_3O_3$ 364.0219; Found: 364.0780 $[M + H]^+$.

IR (KBr), ν, cm^{-1} = 1765, 1731 (2x C=O), 1611 (C=N).

3-(6-bromo-2-oxobenzo[d]oxazol-3(2H)-yl)-N-(2,5-dimethyl-1H-pyrrol-1-yl)propanamide (**15**)

To a solution of hydrazide **6** (0.40 g, 1.3 mmol) in propan-2-ol (25 mL), hexane-2,5-dione (0.45 g, 3,9 mmol) and acetic acid (0.5 mL) were added, and the mixture was refluxed for 18 h. The mixture was cooled down and left for 4 h to crystallize at 4 °C. The formed precipitate was filtered off, washed with propan-2-ol, and dried. The obtained solid was recrystallized from the mixture of propan-2-ol (35 mL) and 1,4-dioxane (15 mL).

White solid, yield 0.23 g (47%), m.p. 205–207 °C.

^{1}H NMR (400 MHz, DMSO-d_6), δ: 1.67–1.80 (m, 3H, CH_3), 2.25–2.43 (m, 3H, CH_3), 2.63–2.75 (m, 0.66H, CH_2), 2.84–2.95 (t, J = 6.3 Hz, 1.34H, CH_2), 3.98–4.12 (m, 2H, CH_2), 7.19–7.30 and 7.36–7.44 and 7.56–7.68 (3m, 5H, H_{arom}), 10.05 and 10.17 (2s, 1H, NH).

^{13}C NMR (101 MHz, DMSO-d_6), δ: 16.12, 16.28 (2CH_3), 34.35 (CH_2-C), 38.61 (N-CH_2), 111.02, 111.27, 112.80, 113.36, 126.46, 130.59, 142.55, 152.61, 153.21, 156.95 (C_{arom}), 165.95, 171.98 (2x C=O).

HRMS (ESI): m/z calcd. for $C_{16}H_{16}BrN_3O_3$ 378.0375; Found: 378.0942 $[M + H]^+$.

IR (KBr), ν, cm^{-1} = 3188 (NH), 1775, 1662 (2x C=O).

1-(3-(6-bromo-2-oxobenzo[d]oxazol-3(2H)-yl)propanamido)-5-oxopyrrolidine-3-carboxylic acid (**16**)

Hydrazide **6** (2 mmol, 0.62 g) was dissolved in water (10 mL) and then itaconic acid (3 mmol, 0.39 g) was added. The mixture was refluxed for 24 h. The formed precipitate was filtered and washed with hot water and dried. The compound **16** was purified by dissolution in 10% Na_2CO_3, filtration, and acidification of the filtrate with acetic acid to pH 5–6. The precipitated crystals were filtered and washed with water and hexane.

White solid, yield 0.77 g (93%), m.p. 203–205 °C.

^{1}H NMR (400 MHz, DMSO-d_6), δ: 2.40–2.47 (m, 1H, O=C-C$\underline{H}_2$-CHCOOH), 2.61 (m, 1H+2H, O=C-C$\underline{H}_2$-CHCOOH + NCH_2C$\underline{H}_2$), 3.25 (t, J = 8.0 Hz, 1H, C$\underline{H}$OOH), 3.45 (t, J = 7.4 Hz, 1H, N-C$\underline{H}_2$-CHOOH), 3.54 (t, J = 8.8 Hz, 1H, N-C$\underline{H}_2$-CHOOH), 4.03 (t, J = 6.9 Hz, 2H, NC$\underline{H}_2$CH_2), 7.26 (d, J = 8.2 Hz, 1H, H_{arom}), 7.40 (d, J = 8.3 Hz, 1H, H_{arom}), 7.64 (s, 1H, H_{arom}), 10.21 (s, 1H, NH), 12.65 (s, 1H, OH).

^{13}C NMR (101 MHz, DMSO-d_6), δ: 30.98, 31.17, 34.02, 38.30 ($\underline{C}H_2$-C, O=C-$\underline{C}H_2$-CHCOOH, N-$\underline{C}H_2$-CHCOOH), 49.35 (N-CH_2), 111.15, 112.86, 113.46, 126.52, 130.47, 142.61 (C_{arom}), 153.24, 168.47, 170.66, 173.99 (4x C=O).

HRMS (ESI): m/z calcd. for $C_{15}H_{14}BrN_3O_6$ 412.0066; Found: 412.0618 $[M + H]^+$.

IR (KBr), ν, cm^{-1} = 3203 (OH), 3010 (NH), 1760, 1696, 1683, 1615 (4x C=O).

6-bromo-3-(2-(5-thioxo-4,5-dihydro-1,3,4-oxadiazol-2-yl)ethyl)benzo[d]oxazol-2(3H)-one (**17**)

The mixture of methanol (20 mL) and KOH (15 mmol, 0.84 g) was stirred at 40 °C. After KOH dissolved CS_2 (10 mmol, 0.77 g, dropwise) was added and the mixture was stirred at room temperature for 20 min. The solution of hydrazide was prepared by dissolving hydrazide (5 mmol, 1.50 g) in methanol (40 mL). The hydrazide solution (dropwise) was added to the primary solution and refluxed for 17 h. The mixture was cooled down, and hydrochloric acid was added dropwise until the pH reached 1. The residue was filtered off and washed with water. The obtained solid was recrystallized from the mixture of propan-2-ol (60 mL) and 1,4-dioxane (6 mL).

White solid, yield 1.06 g (62%), m.p. 205–207 °C.

^{1}H NMR (400 MHz, DMSO-d_6), δ: 3.18 (t, J = 6.6 Hz, 2H, CH_2), 4.18 (t, J = 6.7 Hz, 2H, CH_2), 7.33 (d, J = 8.4 Hz, 1H, H_{arom}), 7.43 (d, J = 8.4, 1H, H_{arom}), 7.67 (s, 1H, H_{arom}), 14.34 (s, 1H, NH).

^{13}C NMR (101 MHz, DMSO-d_6), δ: 23.60 ($\underline{C}H_2$-C), 38.34 (N-CH_2), 110.91, 113.07, 113.74, 126.64, 130.09, 142.58 (C_{arom}), 153.24 (C=O), 161.31 (O-C=N), 177.78 (C=S).

HRMS (ESI): m/z calcd. for $C_{11}H_8BrN_3O_3S$ 342.1670; Found: 342.0017 $[M + H]^+$.

IR (KBr), ν, cm^{-1} = 3225 (NH), X 1632 (C=N), 1158 (C=S).

3-(6-bromo-2-oxobenzo[d]oxazol-3(2H)-yl)-N′-(3-oxoindolin-2-ylidene)propanehydrazide (**18**)

To a hot solution of hydrazide **6** (0.30 g, 1 mmol) in propan-2-ol (15 mL), isatine (0.19 g, 1,3 mmol) was added, and the mixture was heated at reflux for 3 h and then cooled down. The precipitate was filtered off, washed with propan-2-ol, and dried. The obtained solid was recrystallized from the mixture of propan-2-ol (40 mL) and 1,4-dioxane (5 mL).

Yellow solid, yield 0.35 g (80%), m.p. 221–223 °C.

^{1}H NMR (400 MHz, DMSO-d_6), δ: 3.01–3.28 (m, 2H, CH_2), 4.14 (t, J = 7.0 Hz, 2H, CH_2), 6.84–6.95 (m, 1H, H_{arom}), 6.96–7.10 (m, 1H, H_{arom}), 7.29–7.47 (m, 3H, H_{arom}), 7.62 (s, 1H, H_{arom}), 7.88–8.11 (m, 1H, H_{arom}), 10.78 (s, 1H, NH), 11.23 (s, 1H, NH).

^{13}C NMR (101 MHz, DMSO-d_6), δ: 25.51 ($\underline{C}H_2$-C), 37.86 (N-CH_2), 111.30, 112.85, 113.46, 115.16, 121.63, 126.04, 126.51, 130.52, 130.55, 131.58, 142.37, 142.62 (C_{arom}), 143.75 (C=N), 153.25, 162.37, 164.51 (3C=O).

HRMS (ESI): m/z calcd. for $C_{18}H_{13}BrN_4O_4$ 429.0120; Found: 429.0651 $[M + H]^+$.

IR (KBr), ν, cm^{-1} = 3181, 3070 (2x NH), 1769, 1728, 1694 (3x C=O), 1602 (C=N).

2.2. Preparation of Bacterial Cultures

The bacterial strains used in this study were obtained from the American Type Culture Collection (ATCC) and included the Gram-positive cocci *Staphylococcus aureus* subsp. *aureus* (ATCC 9144) and methicillin-resistant *S. aureus* (MRSA, ATCC 43300), the Gram-positive spore-forming rod *Bacillus subtilis* (ATCC 6051), and the Gram-negative rods *Escherichia coli* (ATCC 8739) and *Pseudomonas aeruginosa* (ATCC 10145). All strains were cultured on tryptic soy agar (TSA; Liofilchem, Teramo, Italy) for 24 h at 37 °C prior to use in the disc agar diffusion assay, as well as for determination of minimal inhibitory concentration (MIC), minimal bactericidal concentration (MBC), growth curves, and time–kill assays. Several well-isolated colonies from each culture were suspended in sterile saline to achieve a turbidity equivalent to 0.5 McFarland units. Working suspensions at an approximate concentration of 6 $\log_{10}$ CFU/mL were prepared for antibacterial testing.

2.3. Disc Agar Diffusion Assay

Compounds were initially screened to exclude those lacking antibacterial activity and to identify bacterial strains resistant to the synthesized derivatives. Antibacterial activity was evaluated using the disc agar diffusion assay in accordance with the Clinical and Laboratory Standards Institute (CLSI) guidelines [48].

For the disc diffusion test, bacterial suspensions were prepared by selecting 3–5 colonies from 18–24 h tryptic soy agar TSA cultures. The suspensions were adjusted to a 0.5 McFarland standard, corresponding to approximately 1.5 × 10^8 CFU/mL, and subsequently used for antibacterial testing [49].

Müller–Hinton agar (MHA) (Liofilchem, Roseto degli Abruzzi, Italy) plates were inoculated with the bacterial suspensions. Sterile 6 mm paper discs were impregnated with 5 µL of the tested compounds and placed on the inoculated agar surfaces. Plates were incubated at 37 °C for 24 h. Ciprofloxacin (KRKA, Novo Mesto, Slovenia) at a concentration

of 10 μg/disc served as a positive control. All assays were performed in triplicate, and mean inhibition zone diameters with ± standard deviations (SD) were calculated.

Inhibition zones were measured using a digital caliper (Mitutoyo, Kawasaki, Japan). Compounds producing inhibition zones larger than 8 mm were considered active and were subsequently subjected to further antibacterial evaluation. These compounds were further assessed for their antibacterial potential by determining bacterial growth curves, performing time–kill assays, and conducting cytotoxicity testing.

2.4. Determination of MIC and MBC

The minimum inhibitory concentration (MIC) and minimum bactericidal concentration (MBC) were determined using the microdilution method described by Balouiri et al. (2016) [49]. Serial two-fold dilutions of the tested compounds were prepared in 96-well microplates, ranging from 1:2 to 1:128. Each well was inoculated with a bacterial suspension containing approximately 5×10^4 CFU, previously diluted 1:150 in Müller–Hinton broth (MHB). Ciprofloxacin (KRKA, Slovenia) at a concentration of 0.45 μg/mL served as the positive antibacterial control. The Petri plates were incubated at 37 °C for 24 h. Following incubation, the MIC was defined as the lowest concentration of the compound that completely inhibited visible bacterial growth. To determine the MBC, aliquots from wells showing no visible growth were subcultured onto Mueller–Hinton agar (MHA) plates and incubated at 37 °C for 24 h. The MBC was defined as the lowest concentration producing a ≥99.9% reduction in viable bacterial count relative to the initial inoculum. All experiments were performed in triplicate.

2.5. Growth Curve Assay

The growth kinetics of *Staphylococcus aureus* subsp. *aureus* (ATCC 9144) and methicillin-resistant *S. aureus* (MRSA; ATCC 43300) in response to compounds **9a**, **11**, **12**, and **13** were evaluated following the methodology described by [50], with slight modifications. A single colony from a tryptic soy agar (TSA; Liofilchem, Teramo, Italy) plate was inoculated into Mueller–Hinton broth (MHB; Liofilchem, Roseto degli Abruzzi, Italy) and incubated at 37 °C for 18 h with orbital shaking at 200 rpm. The overnight cultures were then diluted in fresh MHB to achieve an initial optical density at 600 nm (OD_{600}) of 0.05.

Twofold serial dilutions of each test compound were prepared in MHB within the wells of a 96-well flat-bottom microplate (Thermo Fisher Scientific, Nunc, Rochester, NY, USA). An equal volume of bacterial inoculum was added to each well, resulting in final compound concentrations of 125, 62.5, 31.25, 15.6, 7.8, 3.9, and 1.95 μg/mL. Ciprofloxacin (KRKA, Slovenia) at 0.5 μg/mL served as the positive control antibiotic. Wells containing only bacterial inoculum and MHB were included as growth controls, while wells with MHB alone served as blanks for background correction.

The microplates were incubated at 37 °C for 24 h with orbital shaking at 200 rpm. Optical density (OD_{600}) was measured at 1, 2, 3, 4, 5, 6, 7, 8, 20, and 24 h using a Multiskan™ FC Microplate Photometer (Thermo Fisher Scientific, SkanIt, Rocherster, NY, USA). All assays were performed in duplicate, and growth curves were generated by plotting OD_{600} values against time to assess the effects of each compound on bacterial growth dynamics [51].

2.6. Time—Kill Assay

For this study, a single compound and a single pathogen were selected based on the results of the disk diffusion assay. Time–kill kinetics were evaluated using the macrodilution method according to CLSI guidelines, as described previously [52]. *Staphylococcus aureus* (ATCC 9144) was cultured on TSA plates overnight at 37 °C. The following day, a single colony was inoculated into MHB and incubated for 16 h at 37 °C with orbital shaking at

200 rpm. The turbidity of the resulting culture was adjusted to 0.5 McFarland standard using phosphate-buffered saline (PBS).

The suspension was further diluted in MHB, and compound **11** was added at a concentration corresponding to the previously determined MIC, resulting in a final volume of 10 mL and a bacterial concentration of approximately 1×10^6 CFU/mL. A suspension containing *S. aureus* in MHB without compound **11** served as the growth control. Test tubes were incubated for 6 h at 37 °C with orbital shaking at 200 rpm.

At 0, 1, 2, 3, 4, 5, and 6 h, 50 µL aliquots were collected and serially diluted tenfold in MHB. From each dilution, 100 µL was spread onto Mueller–Hinton agar plates (Liofilchem, Italy) using a sterile spreader. Plates were incubated for 24 h at 37 °C, after which viable colonies were counted, and bacterial viability was expressed as $\log_{10}$ CFU/mL. All assays were performed in triplicate.

2.7. Cytotoxicity Assay

The cytotoxicity of compounds **9a**, **11**, **12**, and **13** was evaluated on Vero cells (ATCC CCL-81) using the MTT assay [51]. Vero cells were seeded at a density of 1×10^4 cells per well in 96-well plates (TPP, Trasadingen, Switzerland) and incubated in a humidified atmosphere containing 5% CO_2 at 37 °C for 24 ± 1 h. Various concentrations of the compounds (125, 62.5, 31.25, 15.6, 7.8, 3.9, and 1.95 µg/mL) were prepared in DMEM containing 2% PBS and added to the wells. The plates were then incubated for 72 h. Each concentration was tested twice in quadruplicate.

After 72 h, cell morphology in each well was examined microscopically using an inverted optical microscope (DMiL, Leica, Wetzlar, Germany) equipped with a 3.1 MP camera (Optikam Pro 3, Optika, Ponteranica, Italy) at 10 × 10 magnification.

Subsequently, 10 µL of MTT reagent (5 mg/mL, Sigma-Aldrich, St. Louis, MO, USA) was added to each well, and the cells were incubated for 4 h at 37 °C. Following incubation, the medium was removed, and 100 µL of dimethyl sulfoxide (DMSO, Carl Roth, Karlsruhe, Germany) was added to each well. The plates were then shaken for 5 min, and the optical density of each well was measured using a microplate reader (Multiskan™ FC Microplate Photometer, Thermo Scientific SkanIt, Waltham, MA, USA).

The absorbance of the purple formazan product was recorded at 570 nm, which corresponds to the primary wavelength proportional to the number of viable cells. A reference wavelength of 620 nm was used to correct non-specific absorbance caused by the microplate or other components in the wells. The percentage of cell survival was subsequently calculated, followed by the construction of dose–response curves to determine the CC_{50} value, defined as the concentration causing 50% cell lysis and death. [53].

CC_{50} and MIC values were compared and used to calculate the therapeutic index of the compounds (CC_{50}/MIC). Therapeutic index (TI) values were interpreted as follows: compounds with TI < 1 were considered unsafe, as their cytotoxic concentrations were lower than the effective antibacterial concentrations; TI values between 1 and 10 indicated limited therapeutic safety, whereas TI > 10 reflected good therapeutic safety (https://pmc.ncbi.nlm.nih.gov/articles/PMC4958397/ (accessed on 29 January 2026)).

2.8. Single-Crystal X-Ray Analysis

Diffraction data were collected at 150 K on a Rigaku, XtaLAB Synergy, Dualflex, HyPix diffractometer (Rigaku Corporation, Tokyo 196-8666, Japan) using monochromated Cu-Kα radiation (λ = 1.54184 Å). The crystal structure was solved using the heavy-atom method [54] and refined with the *olex2.refine* [55] refinement package using Levenberg–Marquardt minimisation. All nonhydrogen atoms were refined in anisotropical approximation. The hydrogen atoms were refined by the riding model with *U*iso(H) = 1.2*U*eq(C). Crys-

tal data: a = 20.0070(3), b = 5.82366(9), c = 26.5802(4) Å, β = 101.220(1)°; V = 3037.78(8) Å^3, Z = 8, μ = 3.798 mm^{-1}, Dcalc = 1.5751 g·cm^{-3}; space group is $P2_1/n$. The final R_1 was 0.0937 ($I > 2\sigma(I)$) and wR_2 was 0.2840 (all data). For further details, see the crystallographic data for this compound deposited at the Cambridge Crystallographic Data Centre. Deposition Number CCDC 2505139 contains the supplementary crystallographic data for this paper. These data are provided free of charge by the joint Cambridge Crystallographic Data Centre and Fachinformationszentrum Karlsruhe Access Structures service. (https://www.ccdc.cam.ac.uk/services/structures (accessed on 29 January 2026)).

3. Results

3.1. Chemistry

There has been growing interest in the synthesis and application of β-amino acids due to their occurrence in biologically active compounds, natural products, and significant derivatives. Both alicyclic and heterocyclic β-amino acids are key components in numerous natural and synthetic bioactive molecules [56,57]. Continuing our work in the field of synthesis and research of amino acids, their derivatives, and cyclization products, in this work, we synthesized various 3-(6-bromo-2-oxo-1,3-benzoxazol-3(2*H*)-yl)propanoic acid derivatives and investigated their antimicrobial activity. In our previous work [58], we synthesized a series of derivatives of compound **1** and investigated their antibacterial activity. In the present study, by introducing a bromo substituent into the benzoxazolinone ring, we aimed to enhance the antibacterial activity of related compounds. The initial acid **2** was obtained by bromination of carboxylic acid **1** (Scheme 1).

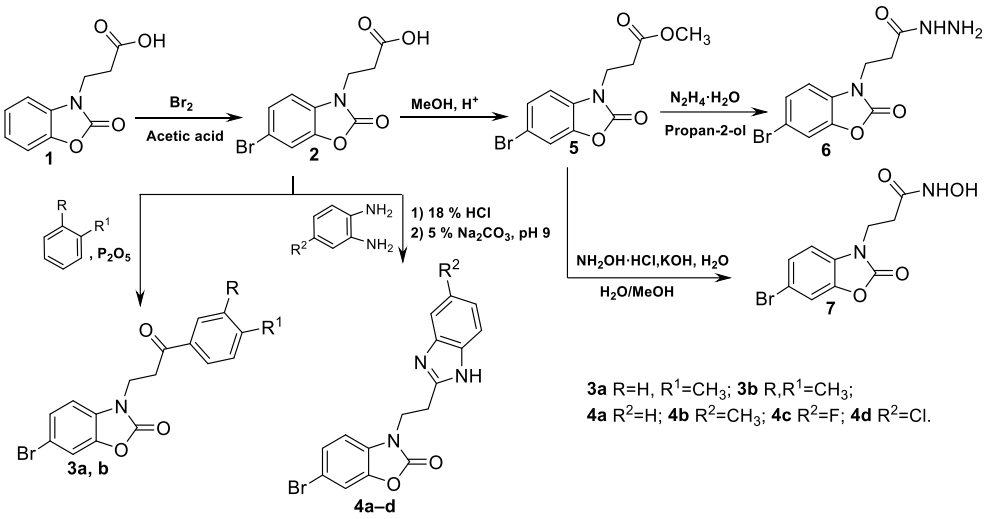

Scheme 1. Synthesis of compounds **1**–**7**.

The resulting acid **2** was expected to be cyclized by boiling its solution in toluene or xylene in a mixture with phosphorus pentoxide. However, structural studies of the resulting compounds revealed that under these conditions, cyclization does not occur, but rather acylation of the aromatic ring occurs and compounds **3a**, **b** are formed. Notably, these compounds were not the initially expected products. To determine their structures, X-ray diffraction analysis was performed, which unambiguously confirmed the identity of 6-bromo-3-(3-oxo-3-(*p*-tolyl)propyl)benzo[d]oxazol-2(3*H*)-one (**3a**). The structures of the compounds **3a** and **3b** were further confirmed by IR, ^{1}H and ^{13}C NMR spectroscopy, and mass spectrometry.

Benzimidazoles have garnered significant research attention due to their diverse therapeutic potentials [59]. Therefore, their exploration was undertaken in our study. The Phillips reaction of compound **2** with a corresponding benzene-1,2-diamines in 18%

hydrochloric acid afforded the scheduled structures **4a**–**e**. The presence of the characteristic benzimidazole multiplets in the aromatic proton region and a broad characteristic singlets observed at 12.34 (**4a**), 12.17 (**4b**), 9.79 (**4c**) and 9.80 (**4d**) ppm confirmed the presence of the benzimidazole NH protons.

To obtain the target acid hydrazide **6**, the conventional synthetic route, carboxylic acid → ester → hydrazide, was employed. Specifically, esterification of carboxylic acid **1** was carried out using methanol in the presence of catalytic sulfuric acid to afford ester **5**, which subsequently underwent hydrazinolysis to yield acid hydrazide **6**. The structures of the intermediate and final products **5** and **6** were confirmed by ^{1}H and ^{13}C NMR spectroscopy, IR spectroscopy, and mass spectrometry. The ^{1}H NMR spectrum of compound **6** displayed two characteristic singlets at δ 9.11 and 4.17 ppm, corresponding to the protons of the $CONHNH_2$ moiety. Three aromatic protons appeared in the range of δ 7.23–7.64 ppm. Additionally, two triplets attributed to the NCH_2CH_2 fragment of the alkyl chain were observed at δ 2.50 and 4.02 ppm, with coupling constants of J = 6.5 Hz and J = 6.7 Hz, respectively. The ^{13}C NMR spectrum of compound **6** showed resonance signals consistent with the expected structure, further confirming the identity of the synthesized molecule.

In the next stage, hydroxamic acid **7** was synthesized by the interaction of ester **5** with hydroxylamine in a mixture of water and methanol 1:1 mixture at 0–5 °C according to the procedure described in [60]. In the ^{1}H NMR spectrum of the synthesized hydroxamic acid, a distinct singlet for the NH proton was observed at 8.79 ppm, along with a singlet for the OH proton at 10.48 ppm.

Numerous hydrazones have been reported, demonstrating a wide range of biological activities [61–66]. Therefore, continuing our work in this area, we synthesized a series of compounds of this class, **8**–**13**. To introduce the hydrazone moiety, hydrazide **6** was reacted with various aromatic and heteroaromatic aldehydes in propan-2-ol under reflux (Scheme 2). The reactions were complete within 3 h, affording the corresponding hydrazones **8**–**13** in yields ranging from 50% to 99%.

NMR analysis revealed that hydrazones **8**–**13** exist in solution (DMSO-d_6) as mixtures of *E*/*Z* rotamers. In all ^{1}H NMR spectra (compounds **8**–**12**, except **8b** and **13**, where CO-NH can be seen as singlets at 11.41 and 11.53 ppm, respectively), the resonances of the N=CH and CO–NH protons appeared as duplicate sets in the ranges 7.75–9.07 ppm and 11.07–11.82 ppm (OH), respectively. The intensity ratio of these signals varied between 0.58:0.42 and 0.72:0.28, depending on the molecular structure. In the ^{13}C NMR spectra, the resonances of the N=CH and CO–NH carbons were observed within the expected intervals. This case of isomerism is described in more detail in the paper [58].

Heterocyclization of 3-(6-bromo-2-oxo-1,3-benzoxazol-3(2*H*)-yl)propanehydrazide (**6**) with diketones gave compounds containing benzoxazolinone-pyrazole (**14**) and benzoxazolinone-pyrrole (**15**) hybrids (Scheme 3). Condensation of acid hydrazide **6** with pentane-2,4-dione in refluxing propan-2-ol in the presence of a catalytic amount of hydrochloric acid yielded the pyrazole derivative **14** in 56% yield. In an analogous procedure, replacement of pentane-2,4-dione with hexane-2,5-dione and the use of catalytic acetic acid furnished the pyrrole derivative **15** in 46% yield. The characteristic NMR signals corresponding to 3,5-dimethylpyrazole and 2,5-dimethylpyrrole moieties were clearly observed, and all spectroscopic and HRMS data were fully consistent with the proposed structures. Investigation of the reaction of hydrazide **6** with itaconic acid has revealed that these primary amines form a compound containing a fragment of γ-amino acid, which undergoes cyclization to the five-membered pyrrolidone cycle **16** already during the reaction (Scheme 3).

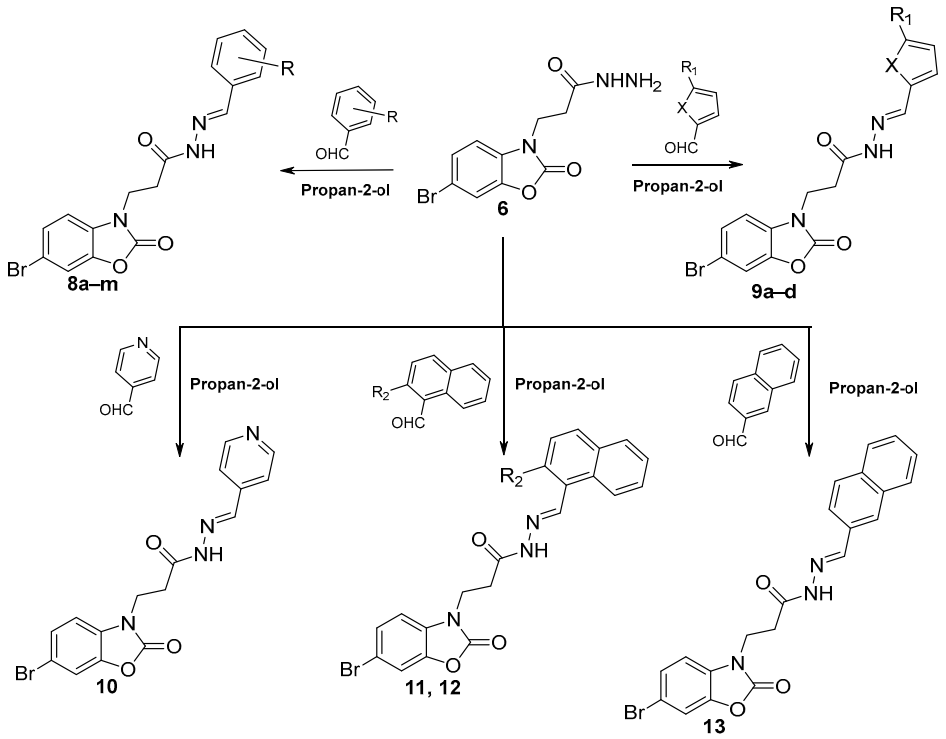

8a R=H; **8b** R=4-CH_3; **8c** R=4-OH; **8d** R=4-F; **8e** R=4-Cl; **8f** R=3-NO_2; **8g** R=4-NO_2; **8h** R=2,4-$(OCH_3)_2$; **8i** R=3,4-$(OCH_3)_2$; **8j** R=2,3,4-$(OCH_3)_3$; **8k** R=3,5-$(CF_3)_2$; **8l** R=4-$N(CH_3)_2$; **8m** R=4-$N(CH_3)_2$; **9a** X=O; R^1=NO_2; **9b** X=S; R^1=H: **9c** X=S; R^1=NO_2; **9d** X=S; R^1=Br; **11** R^2=H; **12** R^2=OH.

Scheme 2. Synthesis of hydrazones **8**–**13**.

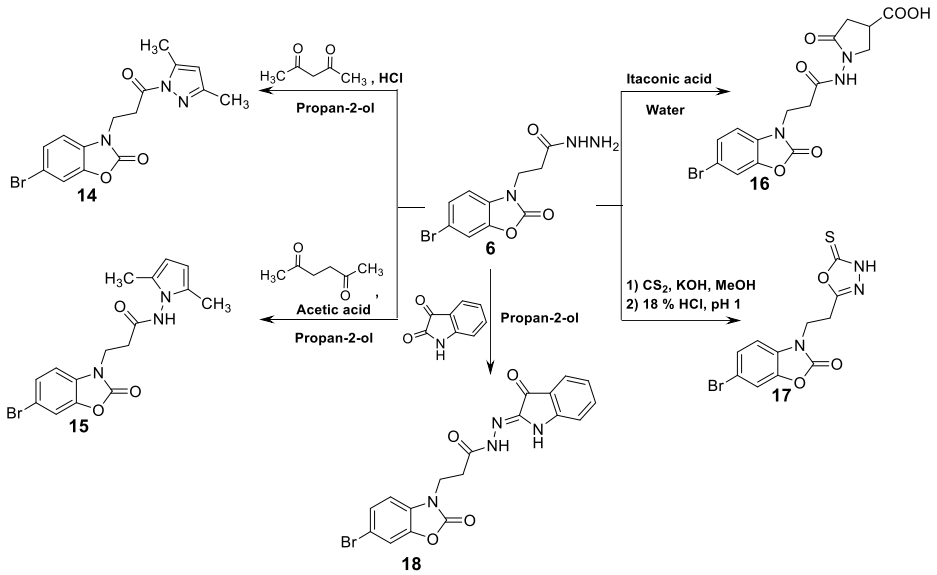

Scheme 3. Synthesis of biheterocyclic compounds **14**–**18**.

Hydrazinocarbonyl compounds undergo reaction with sulphur disulphide in the presence of potassium hydroxide quite easily, and 6-bromo-3-(2-(5-thioxo-4,5-dihydro-1,3,4-oxadiazol-2-yl)ethyl)benzo[*d*]oxazol-2(3*H*)-one (**17**) was synthesized from acid hydrazide **6** according to the method described in the literature [58]. In this ^{1}H NMR spectrum, besides the characteristic proton signals of aromatic and alkyl moieties, the singlet of the NH group proton at 14.34 is observed. ^{1}H NMR analysis indicated that the compound exists exclusively in the thione form in DMSO-d_6 solution, as evidenced by a characteristic singlet at 14.34 ppm corresponding to the NH proton. In the ^{13}C NMR spectrum,

resonances at 153.24 ppm (C=N), 161.31 ppm (C=O), and 177.78 ppm (C=S) confirmed the structural assignment.

Investigation of the reaction of hydrazide **6** with itaconic acid has revealed that these primary amines form a compound containing a fragment of γ-amino acid, which undergoes cyclization to the five-membered pyrrolidone cycle **16** already during the reaction (Scheme 3). At the end of the synthetic work, 3-(6-bromo-2-oxobenzo[*d*]oxazol-3(2*H*)-yl)-*N*′-(3-oxoindolin-2-ylidene)propanehydrazide (**18**) was synthesized via a condensation reaction between isatin and hydrazide **6**, affording the product in 80% yield.

3.2. Evaluation of Antibacterial Activity by the Kirby–Bauer Method

A total of eighteen synthesized chemical compounds (No. **1**–**18**), including several structural analogues (e.g., **3a**, **3b**, **4a**–**4e**, **8a**–**8m**, **9a**–**9d**), were evaluated for their antibacterial properties. The antibacterial activity was assessed using the Kirby–Bauer disk diffusion method, and inhibition zone diameters (mm) were measured against five representative bacterial strains: *S. aureus*, MRSA, *B. subtilis*, *E. coli*, and *P. aeruginosa* (described in the Supplementary Figure S122).

A considerable number of the synthesized compounds (No. **1**–**8**, **9b**–**9d**, **10**, and **13**–**18**) exhibited no detectable inhibitory activity against any of the tested bacterial strains. Since the disk diameter was 6 mm, this area was entirely covered; thus, any potential inhibition smaller than 6 mm could not be observed, making it impossible to determine whether minimal antibacterial effects were present. These findings suggest that most of the synthesized molecules either lack intrinsic antibacterial activity or were tested at concentrations below their effective inhibitory threshold. Only a few compounds demonstrated measurable antibacterial effects against specific bacterial strains (described in the Supplementary Figure S122).

Compound **9a** exhibited moderate antibacterial activity against the Gram-positive rod *B. subtilis*, with an inhibition zone of 12.87 ± 0.35 mm.

Compound **11** showed the highest potency, displaying pronounced inhibitory effects against the Gram-positive cocci *S. aureus* (14.57 ± 0.25 mm) and MRSA (12.14 ± 0.14 mm).

Compound **12** exhibited weak to moderate activity against *S. aureus* (9.42 ± 0.20 mm) and MRSA (9.00 ± 0.17 mm), while remaining inactive against *B. subtilis* and all Gram-negative bacteria.

Compound **13** demonstrated low inhibitory activity against *E. coli* (8.71 ± 0.27 mm) but showed no detectable effect on other tested strains. All other compounds, including the structurally diverse analogues (e.g., **8a**–**8m**), failed to produce measurable inhibition zones against any of the bacterial species tested. Comparison of bacterial susceptibility revealed a clear pattern of selective activity toward Gram-positive cocci. *S. aureus* and MRSA were susceptible to two compounds, whereas the Gram-positive spore-forming bacterium *B. subtilis* and the Gram-negative bacterium *E. coli* were each susceptible to one compound. *P. aeruginosa* exhibited no susceptibility to any of the tested compounds and was therefore excluded from further analysis. This high resistance is consistent with the characteristic structural and functional barriers of Gram-negative bacteria, such as the low permeability of the outer membrane and the presence of efficient efflux pump systems that prevent intracellular accumulation of antibacterial agents.

Ciprofloxacin was used as a positive control to validate the assay conditions. It exhibited strong and broad-spectrum antibacterial activity, producing inhibition zones of 36.00 ± 0.20 mm (*S. aureus*), 32.00 ± 0.27 mm (MRSA), 42.00 ± 0.53 mm (*B. subtilis*), 40.00 ± 0.61 mm (*E. coli*), and 26.00 ± 0.44 mm (*P. aeruginosa*). These results confirm the reliability of the experimental method and the suitability of the setup for accurately determining antibacterial efficacy.

Among all evaluated compounds, only four—**9a**, **11**, **12**, and **13**—displayed measurable antibacterial activity in the Kirby–Bauer disk diffusion assay, predominantly against Gram-positive bacterial strains. Compound **11** demonstrated the greatest potency, effectively inhibiting both methicillin-sensitive and methicillin-resistant *S. aureus*. These results suggest that the tested compounds contain promising structural motifs for the development of new agents targeting Gram-positive pathogens.

3.3. MIC and MBC Evaluation

The minimum inhibitory concentrations (MICs) and minimum bactericidal concentrations (MBCs) of the most active synthesized compounds were determined against representative Gram-positive and Gram-negative bacterial strains, including *S. aureus*, MRSA, *B. subtilis*, and *E. coli.* Ciprofloxacin was used as a reference antibiotic control.

Against *S. aureus*, compound **11** exhibited a MIC value of 31.25 μg/mL and an MBC value of 62.5 μg/mL, while compound **12** showed a MIC of 31.25 μg/mL and an MBC of 125 μg/mL. These results indicate moderate antibacterial activity, with compound **11** displaying slightly stronger bactericidal potential than compound **12.**

For MRSA, compound **11** demonstrated MIC and MBC values of 62.5 μg/mL, suggesting similar inhibitory and bactericidal thresholds. In contrast, compound **12** was more potent, with a MIC of 7.8 μg/mL and an MBC of 62.5 μg/mL, indicating relatively higher inhibitory activity but requiring a greater concentration for bactericidal action.

The reference antibiotic ciprofloxacin exhibited strong activity against both *S. aureus* and MRSA, with MIC/MBC values of 0.125/0.125 μg/mL and 0.25/0.5 μg/mL, respectively, thereby confirming the reliability of the assay conditions.

The spore-forming Gram-positive bacterium *B. subtilis* was tested against compound **9a**, which exhibited strong inhibitory activity, with a MIC of 7.8 μg/mL and an MBC of 62.5 μg/mL, suggesting a pronounced bacteriostatic effect at low concentrations. In comparison, ciprofloxacin showed substantially higher potency, with MIC and MBC values of 0.06 μg/mL and 0.125 μg/mL, respectively.

The Gram-negative bacterium *E. coli* was susceptible only to compound **13**, which showed relatively weak activity, with both MIC and MBC values of 250 μg/mL. This result indicates limited efficacy and suggests that compound **13** exerts minimal bacteriostatic and bactericidal effects against *E. coli*. In contrast, ciprofloxacin displayed high potency, with MIC and MBC values of 0.5 μg/mL, consistent with its known broad-spectrum activity.

Overall, the synthesized compounds exhibited selective antibacterial activity, primarily against Gram-positive bacteria. Compounds **11** and **12** were active against *S. aureus* and MRSA, compound **9a** was effective against *B. subtilis*, and compound **13** showed weak activity against *E. coli*.

In general, the higher MIC and MBC values observed for the synthesized compounds compared with ciprofloxacin indicate moderate antibacterial potency. Nevertheless, their selectivity toward Gram-positive organisms, particularly methicillin-resistant *S. aureus*, suggests that these molecules may serve as promising lead structures for the development of new antibacterial agents targeting resistant staphylococcal infections.

3.4. Correlation Between Disk Diffusion and MIC/MBC

The antibacterial activities of compounds **9a**, **11**, **12**, and **13** were evaluated against *S. aureus*, MRSA, *B. subtilis*, *E. coli*, and *P. aeruginosa*, using ciprofloxacin as a reference standard. The corresponding MIC, MBC, and MBC/MIC values are summarized in Table 1. As shown in the table, the synthesized compounds exhibited variable inhibitory effects, primarily against Gram-positive strains.

Table 1. MIC, MBC, and MBC/MIC values of four compounds against different bacterial species.

Chemical Compounds	Concentrations (μg/mL)	Bacterial Strains				
		S. aureus	MRSA	*B. subtilis*	*E. coli*	*P. aeruginosa*
9a	MIC	NT	NT	7.8	NT	NT
	MBC	NT	NT	62.5	NT	NT
	MBC/MIC	NT	NT	8	NT	NT
11	MIC	31.25	62.5	NT	NT	NT
	MBC	62.5	62.5	NT	NT	NT
	MBC/MIC	NT	NT	NT	NT	NT
12	MIC	31.25	7.8	NT	NT	NT
	MBC	125	62.5	NT	NT	NT
	MBC/MIC	4	8	NT	NT	NT
13	MIC	NT	NT	NT	250	NT
	MBC	NT	NT	NT	250	NT
	MBC/MIC	NT	NT	NT	1	NT
Ciprofloxacin	MIC	0.125	0.25	0.06	0.5	NT
	MBC	0.125	0.5	0.125	0.5	NT

Note: MRSA: Methicillin-resistant *S. aureus*, MIC: minimal inhibitory concentration, MBC: minimal bactericidal concentration, NT—not tested.

Compound **9a** displayed activity exclusively against *B. subtilis* (MIC = 7.8 μg/mL, MBC = 62.5 μg/mL, MBC/MIC = **8**), indicating a predominantly bacteriostatic mode of action.

Compound **11** demonstrated moderate activity against *S. aureus* and MRSA, with MIC values of 31.25 μg/mL and 62.5 μg/mL, respectively.

Compound **12** exhibited the most potent antibacterial effect, inhibiting *S. aureus* (MIC = 31.25 μg/mL) and MRSA (MIC = 7.8 μg/mL) with corresponding MBC/MIC ratios of **4** and **8**, respectively, again suggesting a bacteriostatic effect. The higher susceptibility of MRSA to compound 12 is noteworthy and may reflect favorable structural interactions with bacterial targets associated with resistance mechanisms.

Compound **13** was active only against *E. coli* (MIC = MBC = 250 μg/mL, MBC/MIC = 1), demonstrating a bactericidal effect.

The reference antibiotic ciprofloxacin exhibited potent broad-spectrum activity (MIC = 0.06–0.5 μg/mL), thereby confirming the reliability and validity of the assay conditions.

Overall, these results indicate that the tested compounds display selective antibacterial activity, mainly against Gram-positive bacteria, with compound **12** emerging as the most promising derivative in the series.

3.5. Bacterial Growth Curve Analysis

The antibacterial activities of several synthesized compounds were systematically evaluated against *S. aureus* and MRSA over a 24 h incubation period, with optical density measured at ten time points. Bacterial growth was monitored spectrophotometrically at 600 nm (OD_{600}) at 1, 2, 3, 4, 5, 6, 7, 8, 20, and 24 h, enabling a detailed assessment of growth kinetics and the temporal dynamics of inhibition (Figures 2–9). Ciprofloxacin was used as a positive control, while untreated bacterial cultures served as baseline growth references.

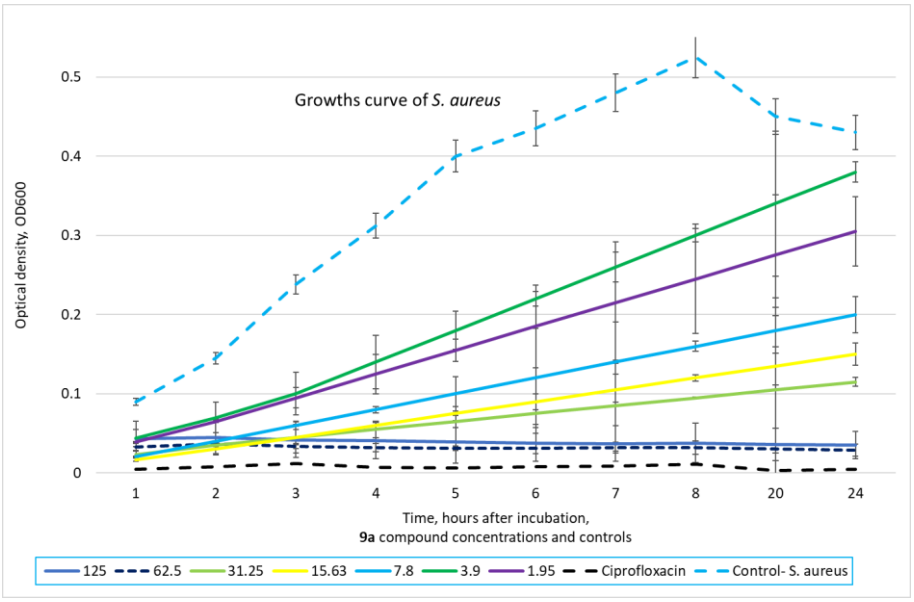

Figure 2. Effect of compound **9a** on the growth of *Staphylococcus aureus* at concentrations ranging from 1.95 to 125 μg/mL. Bacterial growth was monitored by measuring optical density at 600 nm (OD600) at 1, 2, 3, 4, 5, 6, 7, 8, 20, and 24 h after incubation. Values represent mean ± SD (ν = 3).

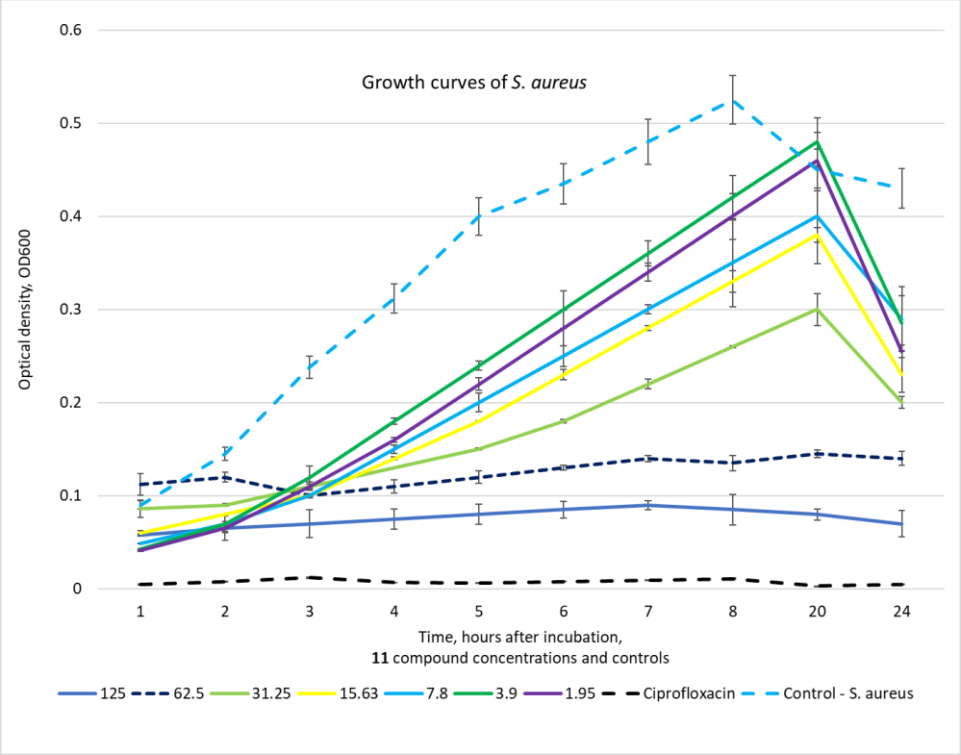

Figure 3. Effect of compound **11** on the growth of *Staphylococcus aureus* at concentrations ranging from 1.95 to 125 μg/mL. Bacterial growth was monitored by measuring optical density at 600 nm (OD600) at 1, 2, 3, 4, 5, 6, 7, 8, 20, and 24 h after incubation. Values represent mean ± SD (ν = 3).

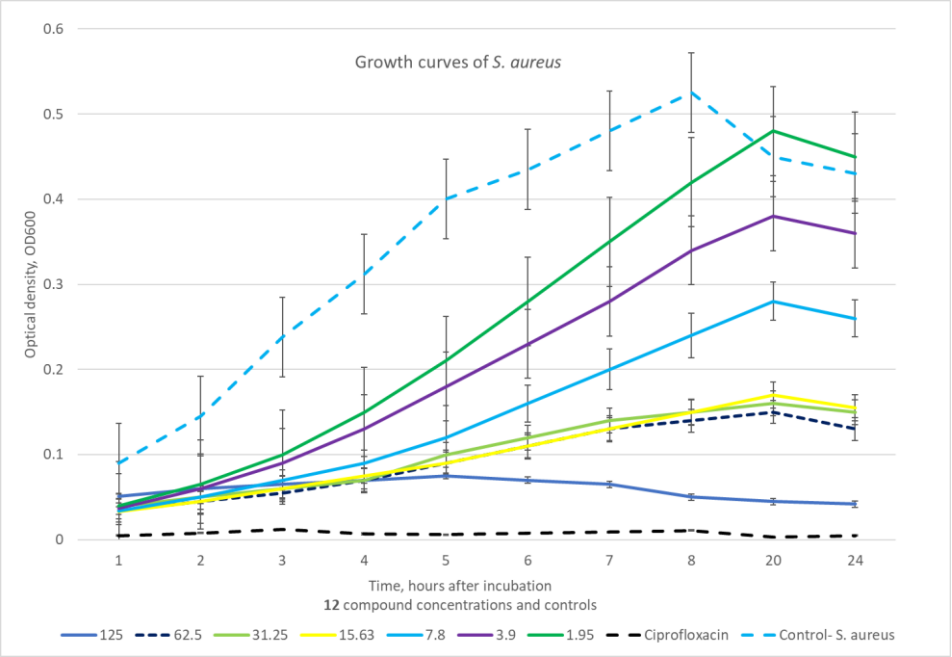

Figure 4. Effect of compound **12** on the growth of *Staphylococcus aureus* at concentrations ranging from 1.95 to 125 µg/mL. Bacterial growth was monitored by measuring optical density at 600 nm (OD600) at 1, 2, 3, 4, 5, 6, 7, 8, 20, and 24 h after incubation. Values represent mean ± SD (ν = 3).

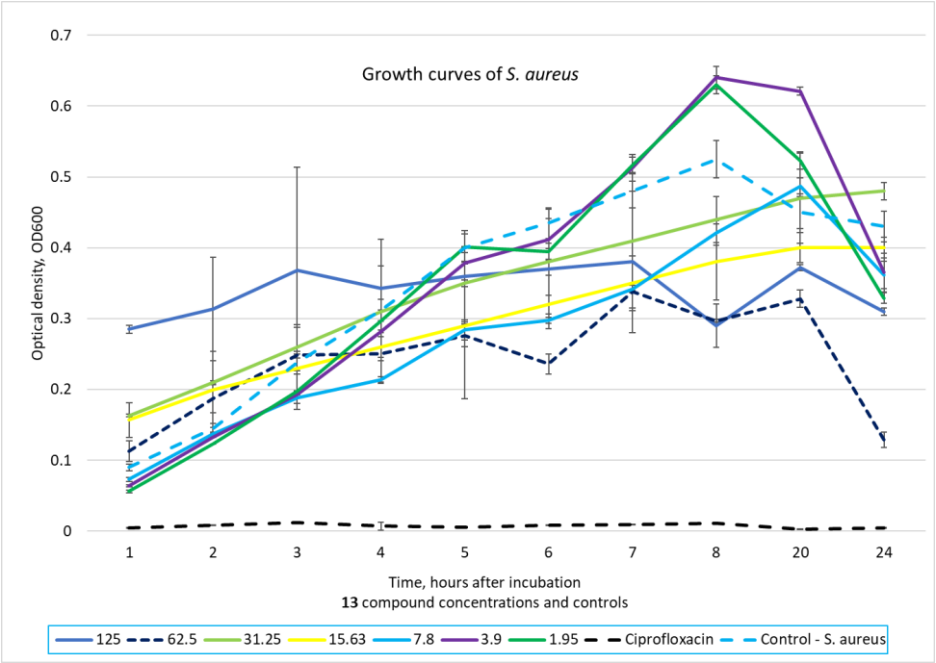

Figure 5. Effect of compound **13** on the growth of *Staphylococcus aureus* at concentrations ranging from 1.95 to 125 µg/mL. Bacterial growth was monitored by measuring optical density at 600 nm (OD600) at 1, 2, 3, 4, 5, 6, 7, 8, 20, and 24 h after incubation. Values represent mean ± SD (ν = 3).

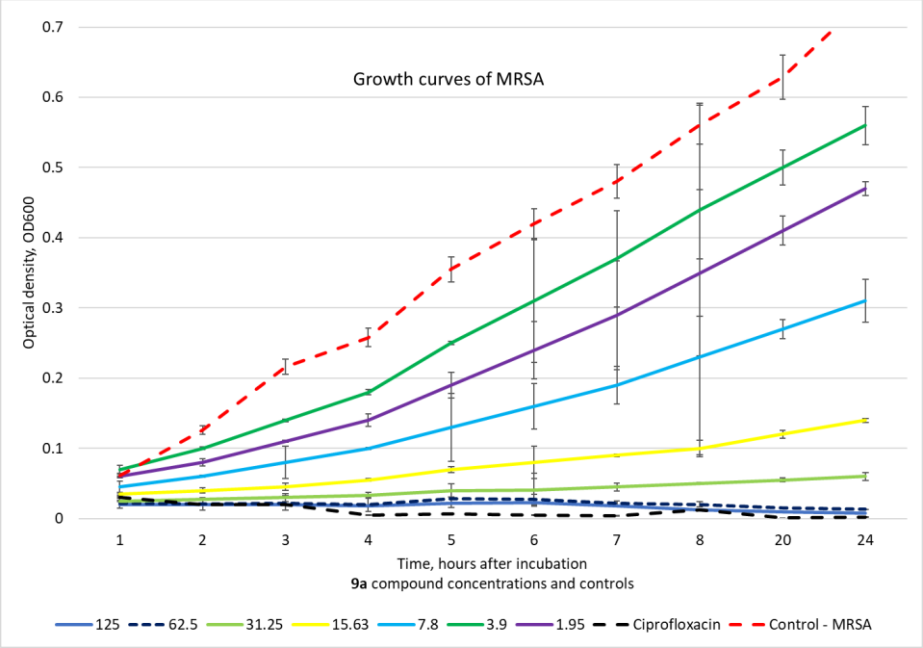

Figure 6. Effect of compound **9a** on the growth of MRSA at concentrations ranging from 1.95 to 125 µg/mL. Bacterial growth was monitored by measuring optical density at 600 nm (OD600) at 1, 2, 3, 4, 5, 6, 7, 8, 20, and 24 h after incubation. Values represent mean ± SD (ν = 3).

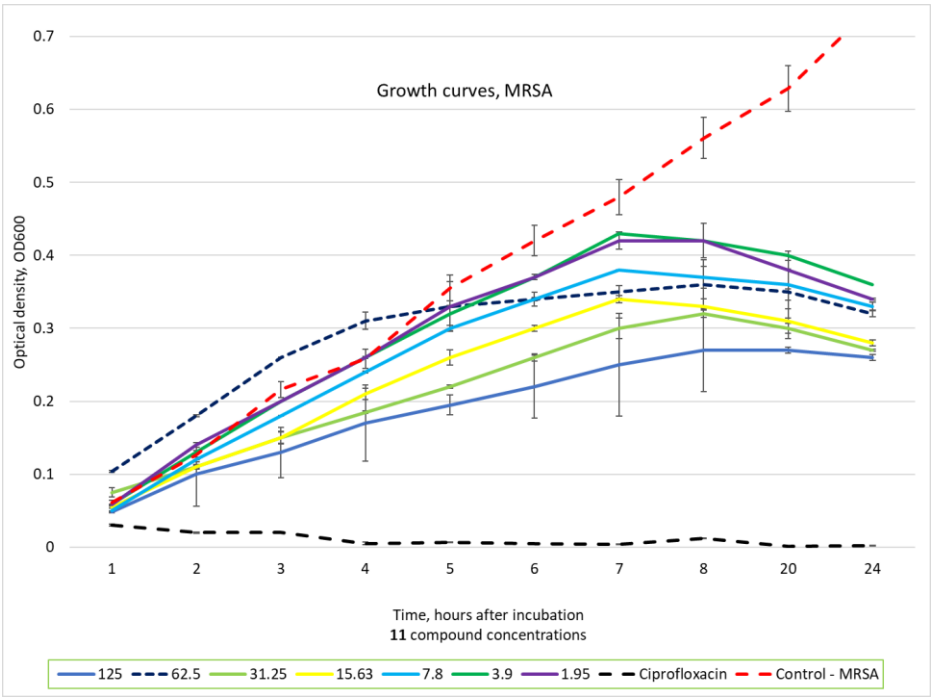

Figure 7. Effect of compound **11** on the growth of MRSA at concentrations ranging from 1.95 to 125 µg/mL. Bacterial growth was monitored by measuring optical density at 600 nm (OD600) at 1, 2, 3, 4, 5, 6, 7, 8, 20, and 24 h after incubation. Values represent mean ± SD (ν = 3).

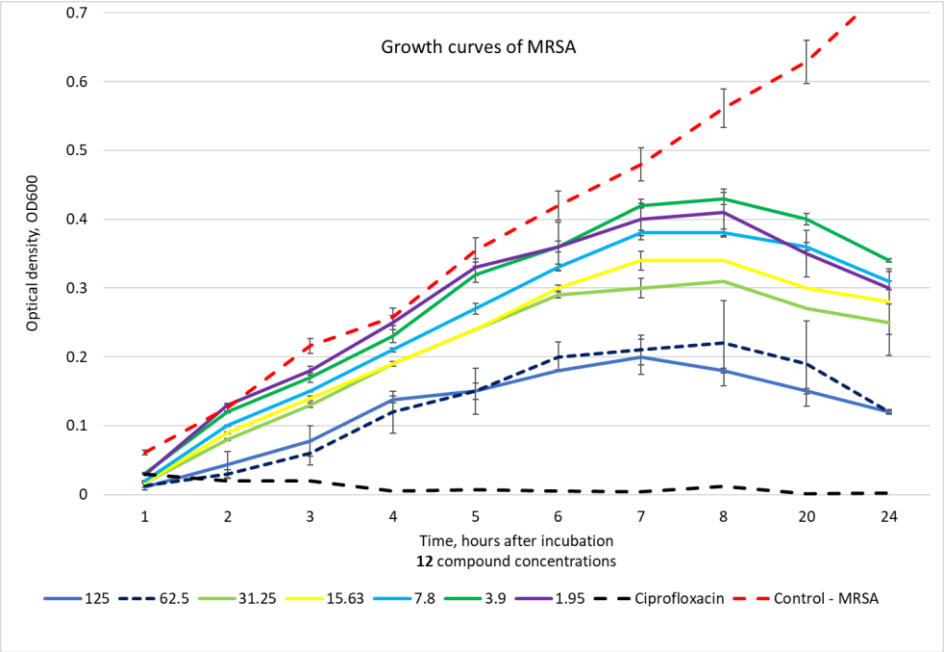

Figure 8. Effect of compound **12** on the growth of MRSA at concentrations ranging from 1.95 to 125 µg/mL. Bacterial growth was monitored by measuring optical density at 600 nm (OD600) at 1, 2, 3, 4, 5, 6, 7, 8, 20, and 24 h after incubation. Values represent mean ± SD (ν = 3).

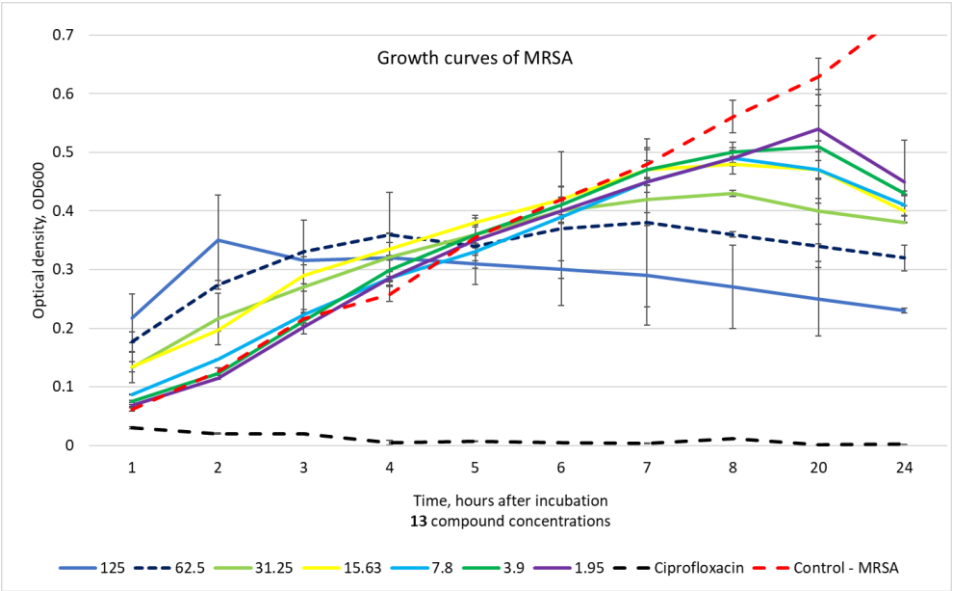

Figure 9. Effect of compound **13** on the growth of MRSA at concentrations ranging from 1.95 to 125 µg/mL. Bacterial growth was monitored by measuring optical density at 600 nm (OD600) at 1, 2, 3, 4, 5, 6, 7, 8, 20, and 24 h after incubation. Values represent mean ± SD (ν = 3).

The compounds exhibited a clear dose-dependent antibacterial effect across all tested samples. At the highest concentration (125 µg/mL), bacterial proliferation was strongly suppressed for both *S. aureus* and MRSA. In the case of compound **13**, elevated OD_{600} readings were observed, particularly at early time points, due to the compound's inherent turbidity. Consequently, part of the measured optical density at high concentrations may reflect solution cloudiness rather than bacterial growth. Nevertheless, overall OD_{600} values remained substantially lower than those of untreated controls, confirming effective inhibition.

The time-dependent inhibition profile varied according to both compound concentration and bacterial strain. At 125 µg/mL, inhibition was apparent from the first hour and

persisted throughout the 24 h, indicating sustained antibacterial activity. At 62.5 μg/mL, partial growth suppression was observed—OD_{600} values gradually increased over time but remained significantly below those of untreated cultures, suggesting slowed, though not completely halted, bacterial proliferation.

At intermediate concentrations (31.25–15.625 μg/mL), bacterial growth resumed progressively after 4–6 h, indicating that inhibitory effects at these levels were transient or limited. Notably, MRSA exhibited a slightly faster recovery compared with *S. aureus*, revealing strain-dependent differences in susceptibility. These findings emphasize that inhibitory effects at sub-maximal concentrations are temporary and that the timing of growth recovery is a critical parameter for assessing compound potency.

At the lowest concentrations (7.8–1.95 μg/mL), bacterial growth closely resembled that of untreated controls, with OD_{600} steadily increasing over the 24 h period. These results confirm that inhibition at such low concentrations was minimal and insufficient for effective bacterial suppression.

Comparison among the tested compounds revealed clear differences in potency. Certain compounds maintained low OD_{600} values across nearly all concentrations, indicating stronger and more sustained antibacterial activity, while others demonstrated only moderate inhibition, particularly against MRSA. Overall, the growth curves show that although several compounds were capable of delaying bacterial proliferation, their inhibitory effects diminished over time at intermediate and lower concentrations.

3.6. Time–Kill Kinetics Against Staphylococcus aureus

The effect of compound **11** on the growth kinetics of *S. aureus* was evaluated by quantifying viable bacterial counts (log_{10} CFU/mL) over a 6 h incubation period, and the results are presented in the time–kill curve (Figure 10). Compound **11** was selected for this experiment because it exhibited the most pronounced antibacterial activity against *S. aureus* in the disk diffusion assay.

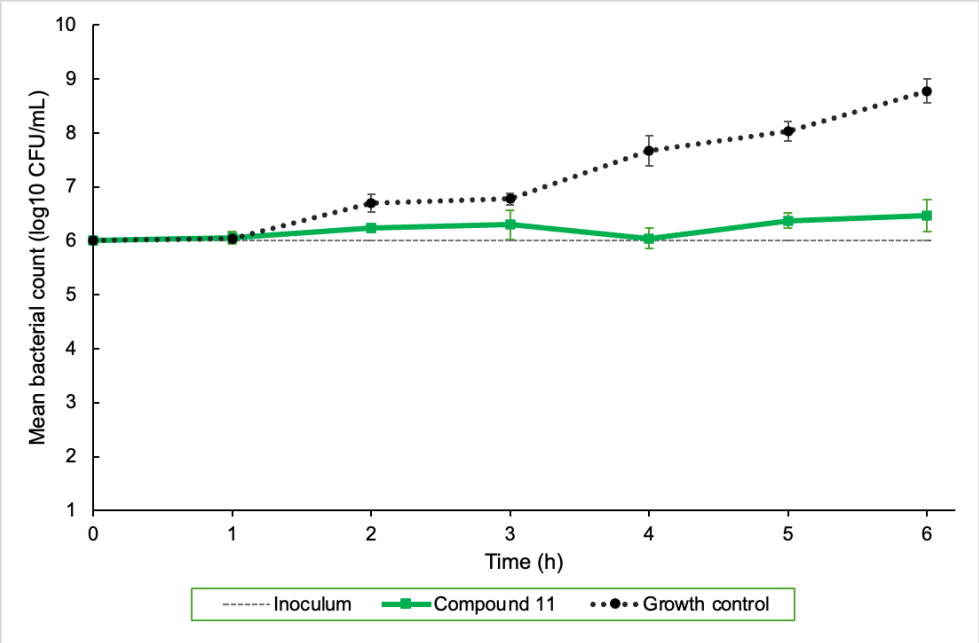

Figure 10. Time–kill kinetics of *Staphylococcus aureus* exposed to compound **11** at a concentration of 31.25 μg/mL. Mean bacterial counts (log_{10} CFU/mL) ± SD from three independent experiments are presented for the growth control (black circles, dotted line) and compound **11**-treated cultures (green squares, solid line). The dashed gray line represents the mean inoculum at 0 h.

At baseline, both the untreated control and the compound **11**–treated cultures had bacterial concentrations of 6.00 $\log_{10}$ CFU/mL ($\pm$ 0.07 and $\pm$ 0.05, respectively). After 1 h, bacterial counts in both groups remained near the initial inoculum, with the control at 6.05 $\pm$ 0.09 $\log_{10}$ CFU/mL (Figure 11a) and the treated culture at 6.06 $\pm$ 0.12 $\log_{10}$ CFU/mL (Figure 11b). These data indicate that during the first hour, untreated *S. aureus* cells were in the adaptation or lag phase, and treatment with compound 11 at 31.25 µg/mL did not cause the death of a significant portion of the population.

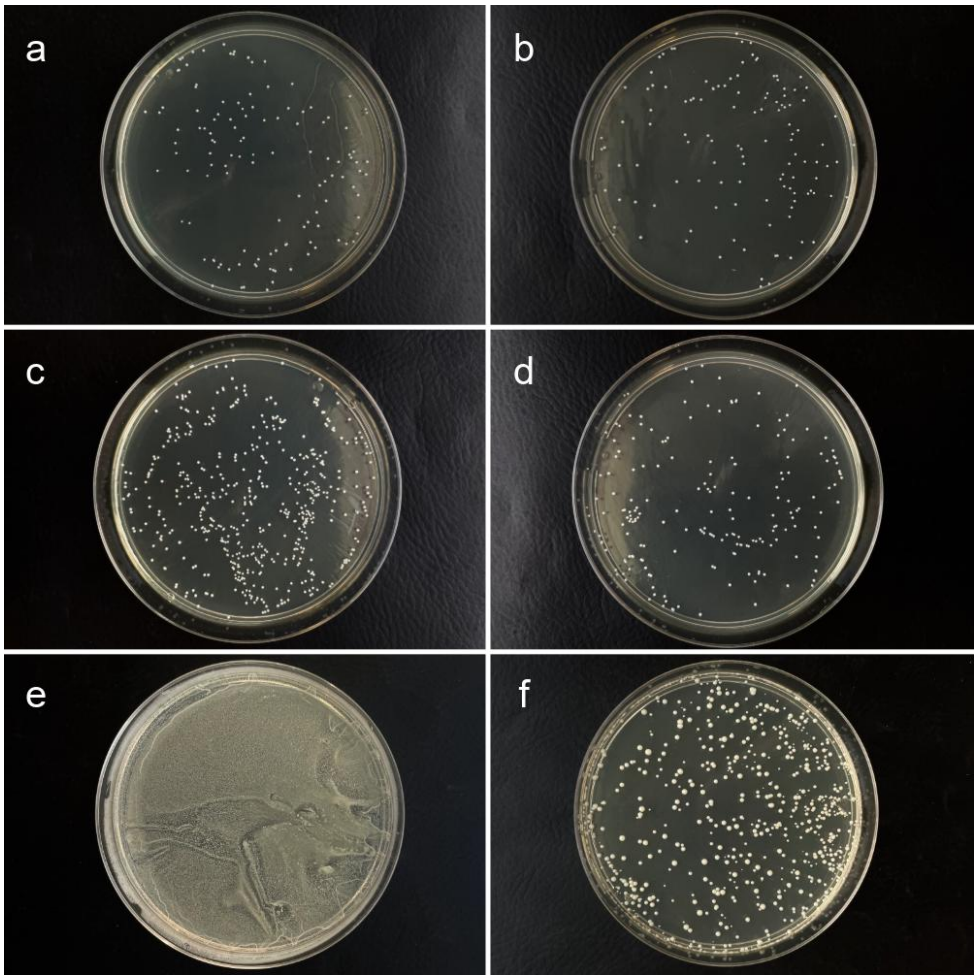

Figure 11. Time–kill effect of compound **11** on *Staphylococcus aureus* growth at different time points. Panels (**a**–**f**) show growth control (**a**,**c**,**e**) and compound-**11**-treated (**b**,**d**,**f**) cultures at **1**, **2**, and **6** h, respectively, plated at a 1:10^3 dilution.

By 2 h, divergence between the groups became apparent ($p < 0.05$): the control increased to 6.70 $\pm$ 0.17 $\log_{10}$ CFU/mL (Figure 11c), whereas the treated culture rose only slightly to 6.23 $\pm$ 0.08 $\log_{10}$ CFU/mL (Figure 11d), indicating the onset of growth inhibition.

After 3 h, both cultures exhibited limited growth, with bacterial counts of 6.78 $\pm$ 0.11 $\log_{10}$ CFU/mL in the control and 6.30 $\pm$ 0.27 $\log_{10}$ CFU/mL in the treated group, maintaining a consistent difference. The most pronounced separation occurred at 4 h: the control reached 7.67 $\pm$ 0.28 $\log_{10}$ CFU/mL, while the treated culture decreased to 6.05 $\pm$ 0.19 $\log_{10}$ CFU/mL, corresponding to a 1.62-$\log_{10}$ reduction relative to the control. These data clearly show that the control bacteria rapidly adapted and transitioned from the lag phase to the log phase within four hours, while the inhibitory effect of compound **11** persisted throughout the entire incubation period.

At 5 h, the control culture increased to 8.04 ± 0.18 $\log_{10}$ CFU/mL, compared with 6.37 ± 0.14 $\log_{10}$ CFU/mL in the treated group, and by 6 h, the control reached 8.78 ± 0.22 $\log_{10}$ CFU/mL (Figure 11e), meanwhile, the culture exposed to compound 11 reached only 6.47 ± 0.29 $\log_{10}$ CFU/mL (Figure 11f).

Quantitatively, the untreated control exhibited bacterial growth over the 6 h experiment (Δ = 2.78 $\log_{10}$ CFU/mL), corresponding to an approximately 600-fold increase in population size, a specific growth rate of 1.07 h^{-1}, a relative growth rate of 190% h^{-1}, and a generation time of approximately 39 min, with growth becoming evident after the initial adaptation phase. Treatment with compound **11** resulted in limited bacterial growth, with counts remaining near the initial inoculum and increasing by only 0.46 $\log_{10}$ CFU/mL over 6 h. This corresponds to a modest 2.9-fold population increase, a specific growth rate of 0.18 h^{-1}, a relative growth rate of 19.3% h^{-1}, and a generation time of approximately 3.9 h.

In summary, these results did not demonstrate that compound **11** at the tested concentration exhibited bactericidal activity under the experimental conditions. However, suppression of *S. aureus* proliferation was evident, resulting in a nearly stable bacterial population throughout the experiment, in contrast to the continuous and robust growth observed in the untreated control.

3.7. Cytotoxicity Evaluation

The cytotoxicity of compounds **9a**, **11**, **12**, and **13** was evaluated at concentrations ranging from 125 to 1.95 μg/mL. The results showed a clear, concentration-dependent decrease in cytotoxicity for all tested compounds.

Vero cells exposed to compounds exhibited distinct morphological changes under microscopic observation (described in the Supplementary Figures S109–S121). The cells lost their typical elongated or polygonal shape and became rounded, shrunken, or irregularly shaped—many cells detached from the culture surface, creating gaps and discontinuities in the monolayer. The cytoplasm appeared granular or vacuolated, indicating intracellular damage. Overall, these changes resulted in a disrupted and sparsely populated cell layer, clearly indicating cytotoxic effects.

The MTT assay confirmed that the compounds **9a**, **11**, **12**, and **13** exhibited cytotoxic effects on Vero cells at concentrations of 125, 62.5, and 31.25 μg/mL (Figure 12). At 15.6 and 7.8 μg/mL, only compound **12** remained cytotoxic. At the lowest concentrations tested (3.9 and 1.95 μg/mL), none of the compounds showed cytotoxicity.

The cytotoxicity of the tested chemical compounds (**9a**, **11**, **12**, and **13**) was determined by measuring their CC_{50} values for subsequent analysis. Among them, compound **12** exhibited the highest cytotoxicity, with the lowest CC_{50} value of 11.7 μg/mL. Compound **9a** showed moderate cytotoxicity (CC_{50} = 19.6 μg/mL), while compounds **13** and **11** were less cytotoxic, with CC_{50} values of 25.7 μg/mL and 29.7 μg/mL, respectively.

At the highest concentration (125 μg/mL), cell viability ranged from 6.8% to 11.4%, indicating strong cytotoxic effects. As the concentration decreased, cell viability increased markedly. For compound **9a**, viability rose from 9.5% at 125 μg/mL to 99.8% at 1.95 μg/mL. Similar trends were observed for compounds **11** (from 11.4% to 99.6%), **12** (from 6.8% to 93.5%), and **13** (from 10.2% to 97.6%).

At concentrations below 7.8 μg/mL, all compounds showed minimal cytotoxicity, maintaining over 90% cell viability, suggesting good biocompatibility at lower doses (Figure 12). These results confirm that the cytotoxic effects of the tested compounds are dose-dependent, with negligible toxicity observed at low concentrations.

The therapeutic indices (TIs) of the tested compounds indicated varying degrees of therapeutic safety. Compound 9a exhibited a TI of 2.5 against *B. subtilis*, suggesting limited therapeutic safety. Compound 11 showed TIs of 0.95 and 0.48 against *S. aureus* and MRSA,

respectively, indicating insufficient therapeutic safety. Compound 12 had TIs of 0.37 and 1.5 for *S. aureus* and MRSA, respectively, reflecting lack of safety against *S. aureus* but limited safety against MRSA. Finally, compound 13 exhibited a TI of 0.1 against *E. coli*, demonstrating very poor therapeutic safety.

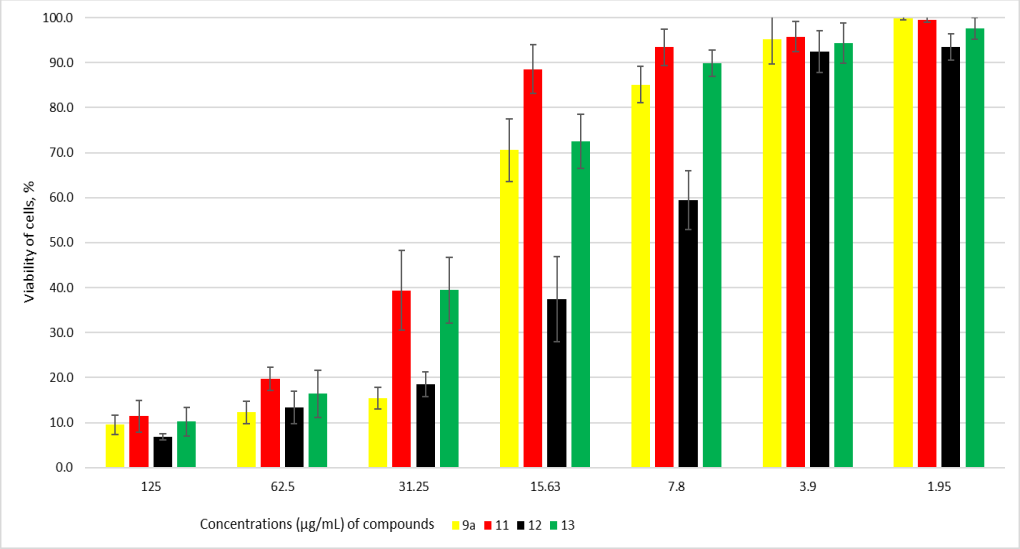

Figure 12. Cell viability after treatment with compounds **9a**, **11**, **12**, and **13** for 72 h on Vero cells. Control sample (untreated cells) = 100% viability. According to the guidelines in ISO 10993-5 (2009) a material concentration is considered non-cytotoxic when cell viability remains above 70%.

3.8. Crystallography

Crystal structure **3a** is characterized by the fact that there are two independent molecules (A and B) in the asymmetric unit. Figure 13 shows an ORTEP view of the asymmetric unit with thermal ellipsoids and the atom-numbering scheme followed in the text. In both independent molecules, the ethane fragments (CH_2CH_2) with benzooxazolone and *p*-methylbenzoyl substituents are characterized by a fully staggered conformation. The torsion angles describing the molecular conformation are slightly different in these molecules (see Table 2).

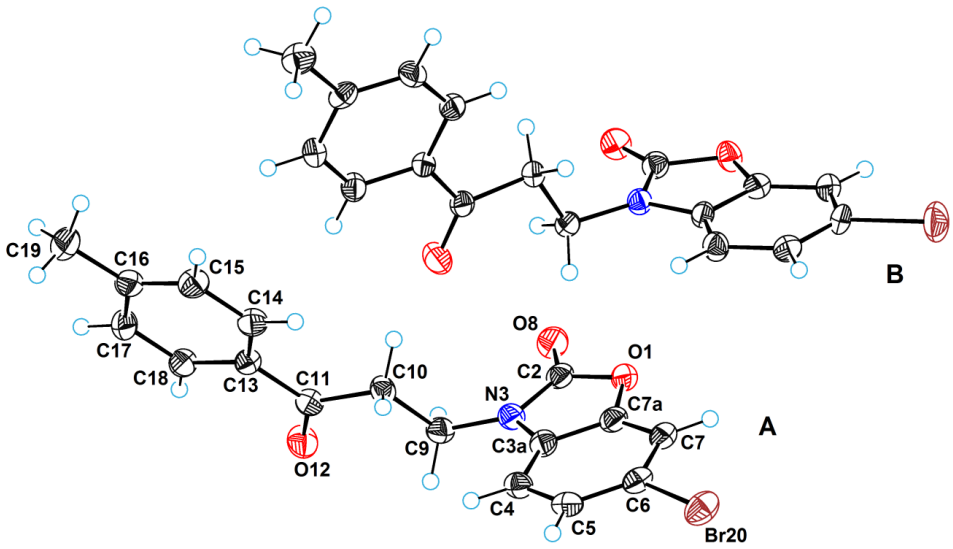

Figure 13. ORTEP diagrams of the asymmetric unit for **3a** with the labels of atoms and molecules.

Table 2. Torsion angles characterizing the conformation of molecules in the crystal structure of **3a**.

Angle	Molecule A	Molecule B
C2-N3-C9-C10	−108.6(8)	−99.9(8)
N3-C9-C10-C11	176.7(8)	−173.8(8)
C9-C10-C11-C13	−174.7(9)	175.6(9)
C10-C11-C13-C14	−9.1(9)	−7.2(9)

The electronegativity of carbon atoms in the ethane fragments is increased due to their bonding with electron acceptor substituents. This leads to the formation of weak and moderate hydrogen bonds of the CH···O type in the crystal structure. Thus, the C10-H group (molecule A) forms an intermolecular hydrogen bond of length 3.19(1) Å with the oxygen atom O12 (molecule B). This bond is designated by the number I (see Figure 14), and given its length, the bond should be considered moderate (its other parameters are H···O = 2.46 Å, C-H···O = 133°). The C9-H group (molecule B) forms an intermolecular hydrogen bond (bond II in Figure 14) with the oxygen atom O1 (molecule A). The parameters of this bond are as follows C···O = 3.22(1) Å, H···O = 2.62 Å, C-H···O = 121°. This bond can also be considered as a CH···π-bond, since the length C···C_S = 3.48 Å (H···C_S = 2.73 Å, C-H··· C_S = 134°, where C_S is the centroid of the oxazole cycle). In addition, this C9-H group also forms a hydrogen bond (bond III in Figure 14) with the O8 atom of another A molecule. The parameters of the bond are following C···O = 3.36(1) Å, H···O = 2.71 Å, C-H···O = 125°. Thusly, the C9-H group participates in a bifurcated hydrogen bond with the O1 atom of the A molecule and the O8 atom of another A molecule. In the crystal structure, there are also other intermolecular hydrogen bonds, which should be considered very weak.

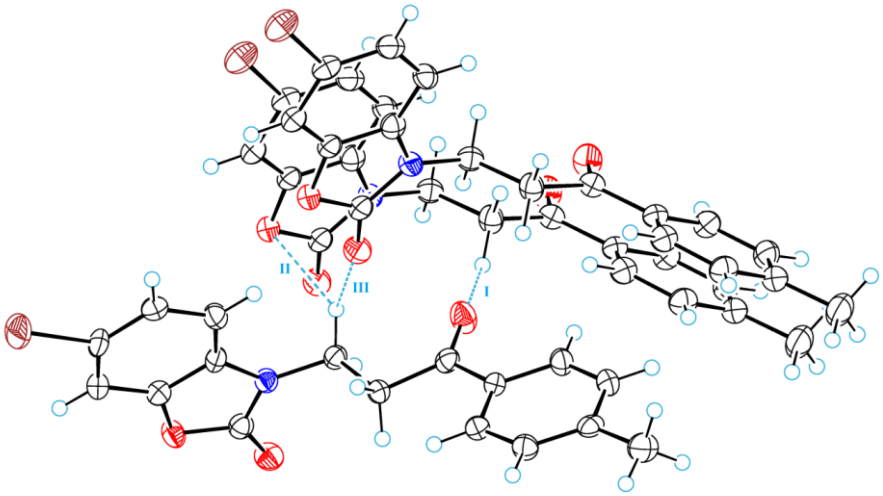

Figure 14. A fragment of molecular packing showing CH···O hydrogen bonds in the crystal structure of **3a**.

Halogen bonds Br···Br with a length of 3.668(7) Å were also detected in the crystal structure. Considering that the van der Waals radius of bromine is 1.95 Å [67], it can be concluded that these halogen bonds are quite strong. Through these bonds, molecular chains are formed from A molecules along the monoclinic axis (see Figure 15).

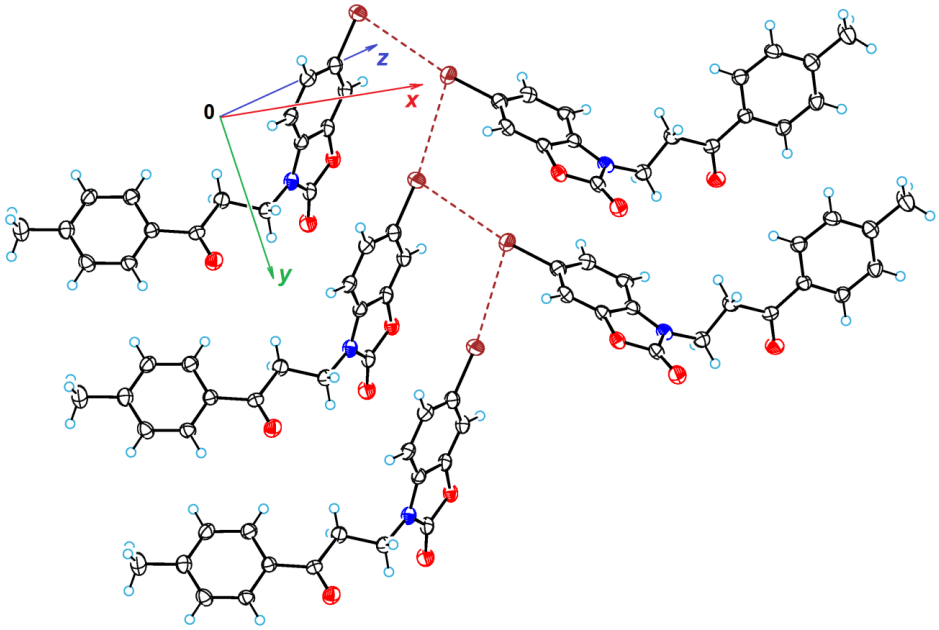

Figure 15. A halogen-bonded molecular chain in the crystal structure of **3a**.

4. Conclusions

In this work, a series of new derivatives of 3-(6-bromobenzoxazolonyl-3)propanoic acid—methyl ester, hydrazide, hydroxamic acid, hydrazones with aromatic and heterocyclic fragments were synthesized. An attempt was made to cyclize 3-(6-bromobenzoxazolonyl-3)propanoic acid to the corresponding tricyclic compound with phosphorus pentoxide in aromatic solvents, but as X-ray structural analysis showed, under these conditions solvent acylation occurred with the formation of 6-bromo-3-(3-oxo-3-(p-tolyl)propyl)benzo[d]oxazol-2(3*H*)-one (**3a**) and 6-bromo-3-(3-(3,4-dimethylphenyl)-3-oxopropyl)benzo[d]oxazol-2(3*H*)-one (**3b**). The corresponding benzimidazole derivatives were obtained by condensation of 3-(6-bromobenzoxazolonyl-3)propanoic acid with *o*-phenylenediamines. Meanwhile, acid hydrazide with diketones formed dimethylpyrrole and dimethylpyrazole derivatives, and under the influence of carbon disulfide, followed by acidification of the intermediate compound with hydrochloric acid, a compound containing an oxothiadiazole ring was synthesized.

The synthesized compounds exhibited selective antibacterial activity predominantly against Gram-positive bacteria. Compounds **11** and **12** demonstrated the highest potency toward *S. aureus*, including MRSA strains, whereas compound **9a** showed activity against *B. subtilis*. Compound **13** exerted only weak inhibition of *E. coli*, and none of the compounds were active against *P. aeruginosa*. This activity profile is consistent with established structural differences in bacterial cell envelopes, as Gram-negative species possess an outer membrane and multiple intrinsic resistance mechanisms that restrict antimicrobial penetration. Disk-diffusion assays, together with MIC and MBC determinations, provided a coherent antibacterial profile for all tested compounds. Compounds **11** and **12** exhibited moderate inhibitory and bactericidal activity, while **9a** acted primarily as a bacteriostatic agent. Compound **13** demonstrated only limited bactericidal effects, in agreement with its minimal inhibition zones in disk-diffusion tests. The strong concordance between MIC/MBC values and disk-diffusion diameters supports the reliability and reproducibility of the methodologies employed. Dynamic growth-curve and time–kill analyses offered further mechanistic insight. The bacterial growth curve analysis can demonstrate the inhibitory effects of different compound concentrations and their duration on bacteria in real time. Growth curve analysis allows interpolation of bacterial concentration, as the

relationship between optical density (OD_{600}) and bacterial count remains linear only for a short period. During our study, bacterial numbers and medium turbidity (OD_{600}) either remained stable or increased, depending on the antibacterial activity of the compounds or the concentrations used. However, OD_{600}-based growth curve analysis does not reveal the percentages of bacterial subpopulations that died or failed to grow or divide, nor how the growth rate was affected, since it is unknown whether the increased turbidity reflects a higher or lower proportion of the initial cell population that survived. Therefore, to accurately assess bactericidal effects, MBC assays and time–kill curve data are necessary.

Compound **11** suppressed *S. aureus* proliferation in a clear dose- and time-dependent manner, showing sustained inhibition at higher concentrations. In contrast, MRSA cultures exhibited faster regrowth at sub-inhibitory concentrations, underscoring strain-specific kinetic responses and the importance of time-dependent assays for identifying potential tolerance or adaptive behaviour.

Comparison of the CC50 values of the compounds **9a**, **11**, **12**, and **13** showed differences of up to threefold. The TIs values obtained for different bacterial species indicated the limited applicability of the tested compounds as standalone antibacterial agents. However, the observed growth suppression suggests that these compounds are worth further investigation as potential adjuvants in combination therapy, enabling dose reduction in conventional antibiotics. Therefore, further studies are warranted to better evaluate their synergistic potential, optimize effective concentrations, and assess their therapeutic relevance in more complex biological models.

Although the therapeutic index is low for systemic application, these compounds may still be suitable for topical or localized use, where higher local concentrations can be achieved with limited systemic exposure.

In conclusion, the tested compounds—particularly **11** and **12**—showed selective antibacterial activity against Gram-positive bacteria, including resistant *S. aureus* strains. Results from disk-diffusion, MIC/MBC, growth-curve, and time–kill assays indicate that compound **11** consistently inhibited bacterial growth under the conditions tested, suggesting it may be a candidate for further investigation as a potential scaffold for future antibacterial development.

Future work should focus on structural optimization to enhance potency, especially against Gram-negative bacteria, clarification of mechanisms of action using molecular and biochemical approaches, and progression to in vivo evaluation to assess pharmacokinetics, efficacy, and safety [68,69].

Supplementary Materials: The following supporting information can be downloaded at: https://www.mdpi.com/article/10.3390/app16042096/s1.

Author Contributions: Conceptualization, J.Š. and V.M.; methodology, M.B. and J.Š.; software, S.B., M.M. and A.Ž.; validation, L.T., R.L. and B.S.-B.; formal analysis, M.B. and V.M.; investigation, M.B., J.Š., B.G. and V.M.; resources, B.G., B.S.-B., L.T.; data curation, J.Š. and V.M.; writing—original draft preparation, M.B. and J.Š.; writing—review and editing, M.B., B.G., B.S.-B. and V.M.; visualization, M.B. and V.M.; supervision, V.M. All authors have read and agreed to the published version of the manuscript.

Funding: This research received no external funding.

Data Availability Statement: The original contributions presented in this study are included in the Supplementary Materials. Further inquiries can be directed to the corresponding author.

Conflicts of Interest: The authors declare no conflicts of interest.

References

1. Jackson, A.C.; Pinter, T.B.J.; Talley, D.C.; Baker-Agha, A.; Patel, D.; Smith, P.J.; Franz, K.J. Benzimidazole and Benzoxazole Zinc Chelators as Inhibitors of Metallo-β-Lactamase NDM-1. *ChemMedChem* **2021**, *16*, 654–661. [CrossRef]
2. McKee, M.L.; Kerwin, S.M. Synthesis, metal ion binding, and biological evaluation of new anticancer 2-(2′-hydroxyphenyl)benzoxazole analogs of UK-1. *Bioorganic Med. Chem.* **2008**, *16*, 1775–1783. [CrossRef] [PubMed] [PubMed Central]
3. Paderni, D.; Giorgi, L.; Voccia, M.; Formica, M.; Caporaso, L.; Macedi, E.; Fusi, V. A New Benzoxazole-Based Fluorescent Macrocyclic Chemosensor for Optical Detection of Zn^{2+} and Cd^{2+}. *Chemosensors* **2022**, *10*, 188. [CrossRef]
4. Hohmann, C.; Schneider, K.; Bruntner, C.; Irran, E.; Nicholson, G.; Bull, A.T.; Jones, A.L.; Brown, R.; Stach, J.E.M.; Goodfellow, M.; et al. Caboxamycin, a new antibiotic of the benzoxazole family produced by the deep-sea strain *Streptomyces* sp. NTK 937. *J. Antibiot.* **2009**, *62*, 99–104. [CrossRef] [PubMed]
5. Cheerala, V.S.K.; Akhir, A.; Saxena, D.; Maitra, R.; Chopra, S.; Neelakantan, S.C.N. Discovery of benzoxazole–thiazolidinone hybrids as promising antibacterial agents against *Staphylococcus aureus* and *Enterococcus* species. *RSC Med. Chem.* **2023**, *14*, 1712–1721. [CrossRef]
6. Ertan, T.; Yildiz, I.; Tekiner-Gülbaş, B.; Bolelli, K.; Temiz-Arpaçi, O.; Özkan, S.; Yalçın, I.; Aki, E. Synthesis, biological evaluation and 2D-QSAR analysis of benzoxazoles as antimicrobial agents. *Eur. J. Med. Chem.* **2009**, *44*, 501–510. [CrossRef]
7. Tekiner-Gulbas, B.; Yildiz-Oren, I.; Temiz-Arpaci, O.; Yalcin, I.; Aki-Sener, E.; Altanlar, N. Synthesis and in vitro antimicrobial activity of new 2-[p-substituted-benzyl]-5-[substituted-carbonylamino]benzoxazoles. *Eur. J. Med. Chem.* **2007**, *42*, 1293–1299. [CrossRef]
8. Klimešová, V.; Kocí, J.; Waisser, K.; Kaustová, J.; Möllmann, U. Preparation and in vitro evaluation of benzylsulfanyl benzoxazole derivatives as potential antituberculosis agents. *Eur. J. Med. Chem.* **2009**, *44*, 2286–2293. [CrossRef]
9. Lu, X.; Hu, X.; Liu, Z.; Zhang, T.; Wang, R.; Wan, B.; Franzblau, S.G.; You, Q. Benzylsulfanyl benzo-heterocycle amides and hydrazones as new agents against drug-susceptible and resistant *Mycobacterium tuberculosis*. *Med. Chem. Commun.* **2017**, *8*, 1303–1310. [CrossRef]
10. Guzow, K.; Mulkiewicz, E.; Obuchowski, M.; Wiczk, W. Biological activity of 3-(2-benzoxazol-5-yl)alanine derivatives. *Amino Acids* **2021**, *53*, 1257–1268. [CrossRef]
11. Zhang, W.; Liu, J.; Macho, J.M.; Jiang, X.; Xie, D.; Jiang, F.; Liu, W.; Fu, L. Design, synthesis and antimicrobial evaluation of novel benzoxazole derivatives. *Eur. J. Med. Chem.* **2017**, *126*, 7–14. [CrossRef]
12. Arslan, G.; Gökçe, B.; Muhammed, M.T.; Albayrak, Ö.; Önkol, T.; Özçelik, A.B. Synthesis, DFT Calculations, and Molecular Docking Study of Acetohydrazide-Based Sulfonamide Derivatives as Paraoxonase 1 Inhibitors. *ChemistrySelect* **2023**, *8*, e202204630. [CrossRef]
13. Šlachtová, V.; Brulíková, L. Benzoxazole derivatives as promising antitubercular agents: A concise review. *ChemistrySelect* **2018**, *3*, 4653–4662. [CrossRef]
14. Reddy, K.I.; Aruna, C.; Sudhakar Babu, K.; Vijayakumar, V.; Manisha, M.; Padma Sridevi, J.; Yogeeswari, P.; Sriram, D. General and efficient synthesis of benzoxazol-2(3H)-ones: Evolution of their anti-cancer and anti-mycobacterial activities. *RSC Adv.* **2014**, *4*, 59594–59602. [CrossRef]
15. Zhou, Y.; Sun, Z.; Zhou, Q.; Zeng, W.; Zhang, M.; Feng, S.; Xue, W. Novel flavonol derivatives containing benzoxazole as potential antiviral agents: Design, synthesis, and biological evaluation. *Mol. Divers.* **2024**, *28*, 3919–3935. [CrossRef] [PubMed]
16. Zhang, N.; Zeng, W.; Zhou, Q.; Sun, Z.; Meng, K.; Qin, Y.; Hu, Y.; Xue, W. Design, Synthesis, Antibacterial and Antiviral Evaluation of Chalcone Derivatives Containing Benzoxazole. *Arab. J. Chem.* **2024**, *17*, 105368. [CrossRef]
17. Hou, Z.; Ling, L.; Wei, J.; Xu, B. Progress in the Prevalence, Classification and Drug Resistance Mechanisms of Methicillin-Resistant *Staphylococcus aureus*. *Infect. Drug. Resist.* **2023**, *16*, 3271–3292. [CrossRef] [PubMed]
18. Sendra, E.; Fernández-Muñoz, A.; Zamorano, L.; Oliver, A.; Horcajada, J.P.; Juan, C.; Gómez-Zorrilla, S. Impact of multidrug resistance on the virulence and fitness of *Pseudomonas aeruginosa*: A microbiological and clinical perspective. *Infection* **2024**, *52*, 1235–1268. [CrossRef]
19. Alasmaria, S.Z.; Makkawia, M.H.; Ahmad, I.; Hakamia, A.R.; Hakami, A.R.; El-Azab, A.S.; Abdel-Aziz, A.A.M.; Ghazwanic, M. Antibacterial evaluation of 2-(6-Chloro-2-p-tolylquinazolin-4-ylthio) acetonitrile against pathogenic bacterial isolates with special reference to biofilm formation inhibition adevindernd anti-adherence properties. *J. King Saud Univ. Sci.* **2024**, *36*, 103316. [CrossRef]
20. Kumar, D.; Jacob, M.R.; Reynolds, M.B.; Kerwin, S.M. Synthesis and evaluation of anticancer benzoxazoles and benzimidazoles related to UK-1. *Bioorg. Med. Chem.* **2002**, *10*, 3997–4004. [CrossRef]
21. El-Ghobashy, N.M.; El-Sayed, S.M.; Shehata, I.A.; El-Ashmawy, M.B. Synthesis, biological evaluation, and molecular modeling studies of new benzoxazole derivatives as PARP-2 inhibitors targeting breast cancer. *Sci. Rep.* **2022**, *12*, 16246. [CrossRef]
22. El-Helby, A.G.A.; Sakr, H.; Eissa, I.H.; Abulkhair, H.; Al-Karmalawy, A.A.; El-Adl, K. Benzoxazole/benzothiazole-derived VEGFR-2 inhibitors: Design, synthesis, molecular docking, and anticancer evaluations. *Arch. Der Pharm.* **2019**, *352*, 1900113. [CrossRef]

23. Elkady, H.; Elwan, A.; El-Mahdy, H.A.; Doghish, A.S.; Ismail, A.; Taghour, M.S.; Elkaeed, E.B.; Eissa, I.H.; Dahab, M.A.; Mahdy, H.A.; et al. New benzoxazole derivatives as potential VEGFR-2 inhibitors and apoptosis inducers: Design, synthesis, anti-proliferative evaluation, flow-cytometric analysis, and in silico studies. *J. Enzyme Inhib. Med. Chem.* **2022**, *37*, 403–416. [CrossRef]
24. Taghour, M.S.; Mahdy, H.A.; Gomaa, M.H.; Aglan, A.; Eldeib, M.G.; Elwan, A.; Dahab, M.A.; Elkaeed, E.B.; Alsfouk, A.A.; Khalifa, M.M.; et al. Benzoxazole derivatives as new VEGFR-2 inhibitors and apoptosis inducers. *J. Enzyme Inhib. Med. Chem.* **2022**, *37*, 2063–2077. [CrossRef] [PubMed]
25. Elwan, A.; Abdallah, A.E.; Mahdy, H.A.; Dahab, M.A.; Taghour, M.S.; Elkaeed, E.B.; Mehany, A.B.M.; Nabeeh, A.; Adel, M.; Alsfouk, A.A.; et al. Modified benzoxazole-based VEGFR-2 inhibitors and apoptosis inducers: Design, synthesis, and anti-proliferative evaluation. *Molecules* **2022**, *27*, 5047. [CrossRef] [PubMed]
26. Osmaniye, D.; Çelikateş, B.K.; Sağlık, B.N.; Levent, S.; Kaplancıklı, Z.A.; Çevik, U.A.; Çavuşoğlu, B.K.; Ilgın, S.; Özkay, Y. Synthesis of some new benzoxazole derivatives and investigation of their anticancer activities. *Eur. J. Med. Chem.* **2021**, *210*, 112979. [CrossRef] [PubMed]
27. Rida, S.M.; Ashour, F.A.; El-Hawash, S.A.; ElSemary, M.M.; Badr, M.H.; Shalaby, M.A. Synthesis of some novel benzoxazole derivatives as anticancer, anti-HIV-1 and antimicrobial agents. *Eur. J. Med. Chem.* **2005**, *40*, 949–959. [CrossRef]
28. Rzeska, A.; Malicka, J.; Guzow, K.; Szabelski, M.; Wiczk, W. New highly fluorescent amino-acid derivatives: Substituted 3-[2-(phenyl)benzoxazol-5-yl]-alanines: Synthesis and photophysical properties. *J. Photochem. Photobiol. A: Chem.* **2001**, *146*, 9–18. [CrossRef]
29. Kuzu, B.; Hepokur, C.; Alagoz, M.A.; Burmaoglu, S.; Algul, O. Synthesis, biological evaluation and in silico studies of some 2-substituted benzoxazole derivatives as potential anticancer agents to breast cancer. *ChemistrySelect* **2022**, *7*, e202103559. [CrossRef]
30. Aiello, S.; Wells, G.; Stone, E.L.; Kadri, H.; Bazzi, R.; Bell, D.R.; Stevens, M.F.G.; Matthews, C.S.; Bradshaw, T.D.; Westwell, A.D. Synthesis of fluorinated 2-aryl benzoxazoles and evaluation against breast cancer cell lines. *J. Med. Chem.* **2008**, *51*, 5135–5139. [CrossRef]
31. Kovács, F.; Huliák, I.; Árva, H.; Kiricsi, M.; Erdős, D.; Kocsis, M.; Takács, G.; Balogh, G.T.; Frank, É. Medicinal-Chemistry-Driven Approach to 2-Substituted Benzoxazole–Estradiol Chimeras: Synthesis, Anticancer Activity, and Early ADME Profile. *ChemMedChem* **2023**, *18*, e202300352. [CrossRef]
32. Afzal, O.; Altamimi, A.S.A.; Shahroz, M.M.; Sharma, H.K.; Riadi, Y.; Hassan, M.Q. Analgesic and anticancer activity of benzoxazole-clubbed 2-pyrrolidinones as novel inhibitors of monoacylglycerol lipase. *Molecules* **2021**, *26*, 2389. [CrossRef] [PubMed]
33. Seth, K.; Garg, S.K.; Kumar, R.; Purohit, P.; Meena, V.S.; Goyal, R.; Banerjee, U.C.; Chakraborti, A.K. 2-(2-Arylphenyl)benzoxazole As a Novel Anti-Inflammatory Scaffold: Synthesis and Biological Evaluation. *ACS Med. Chem. Lett.* **2014**, *5*, 512–516. [CrossRef] [PubMed]
34. Kaur, A.; Pathak, D.P.; Sharma, V.; Wakode, S. Synthesis, biological evaluation and docking study of a new series of di-substituted benzoxazole derivatives as selective COX-2 inhibitors and anti-inflammatory agents. *Bioorg. Med. Chem.* **2018**, *26*, 891–902. [CrossRef] [PubMed]
35. Song, H.; Oh, S.-R.; Lee, H.-K.; Han, G.; Kim, J.-H.; Chang, H.W.; Doh, K.-E.; Rhee, H.-K.; Choo, H.-Y. Synthesis and evaluation of benzoxazole derivatives as 5-lipoxygenase inhibitors. *Bioorg. Med. Chem.* **2010**, *18*, 7580–7585. [CrossRef]
36. Kablaoui, N.; Patel, S.; Shao, J.; Demian, D.; Hoffmaster, K.; Berlioz, F.; Vazquez, M.L.; Moore, W.M.; Nugent, R.A. Novel benzoxazole inhibitors of mPGES-1. *Bioorg. Med. Chem. Lett.* **2013**, *23*, 907–911. [CrossRef]
37. Walker, D.P.; Arhancet, G.B.; Lu, H.-F.; Heasley, S.E.; Metz, S.; Kablaoui, N.M.; Franco, F.M.; Hanau, C.E.; Scholten, J.A.; Springer, J.R.; et al. Synthesis and biological evaluation of substituted benzoxazoles as inhibitors of mPGES-1: Use of a conformation-based hypothesis to facilitate compound design. *Bioorg. Med. Chem. Lett.* **2013**, *23*, 1120–1126. [CrossRef]
38. Arhancet, G.B.; Walker, D.P.; Metz, S.; Fobian, Y.M.; Heasley, S.E.; Carter, J.S.; Springer, J.R.; Jones, D.E.; Hayes, M.J.; Shaffer, A.F.; et al. Discovery and SAR of PF-4693627, a potent, selective and orally bioavailable mPGES-1 inhibitor for the potential treatment of inflammation. *Bioorg. Med. Chem. Lett.* **2013**, *23*, 1114–1119. [CrossRef]
39. Dunwell, D.W.; Evans, D.; Hicks, T.A. 2-Aryl-5-benzoxazolealkanoic acid derivatives with notable anti-inflammatory activity. *J. Med. Chem.* **1975**, *18*, 53–58. [CrossRef]
40. Shakya, A.K.; Kaur, A.; Al-Najjar, B.O.; Naik, R.R. Molecular modeling, synthesis, characterization and pharmacological evaluation of benzo[*d*]oxazole derivatives as non-steroidal anti-inflammatory agents. *Saudi Pharm. J.* **2016**, *24*, 616–624. [CrossRef]
41. Koeberle, A.; Werz, O. Design and development of microsomal prostaglandin E_2 synthase-1 (mPGES-1) inhibitors as a new class of anti-inflammatory drugs. *J. Med. Chem.* **2016**, *59*, 1230–1249. [CrossRef] [PubMed]
42. Geldern, T.W.; Lai, C.; Gum, R.J.; Daly, M.; Sun, C.; Fry, E.H.; Abad-Zapatero, C. Benzoxazole benzenesulfonamides are novel allosteric inhibitors of fructose-1,6-bisphosphatase with a distinct binding mode. *Bioorg. Med. Chem. Lett.* **2006**, *16*, 1807–1811. [CrossRef]

43. Angeli, A.; Peat, T.S.; Bartolucci, G.; Nocentini, A.; Supuran, C.T.; Carta, F. Intramolecular oxidative deselenization of acylselenoureas: A facile synthesis of benzoxazole amides and carbonic anhydrase inhibitors. *Org. Biomol. Chem.* **2016**, *14*, 11353–11356. [CrossRef] [PubMed]
44. Bononi, G.; Tonarini, G.; Poli, G.; Barravecchia, I.; Caligiuri, I.; Macchia, M.; Demontis, G.C.; Minutolo, F.; Rizzolio, F. Monoacylglycerol lipase (MAGL) inhibitors based on a diphenylsulfide-benzoylpiperidine scaffold: Design, synthesis and anticancer evaluation. *Eur. J. Med. Chem.* **2021**, *223*, 113679. [CrossRef]
45. Yang, Z.; Fairfax, D.J.; Maeng, J.H.; Masih, L.; Usyatinsky, A.; Hassler, C.; Isaacson, S.; Fitzpatrick, K.; DeOrazio, R.J.; Chen, J.; et al. Discovery of 2-substituted benzoxazole carboxamides as 5-HT_3 receptor antagonists. *Bioorg. Med. Chem. Lett.* **2010**, *20*, 6538–6541. [CrossRef]
46. Satyendra, R.V.; Vishnumurthy, K.A.; Vagdevi, H.M.; Dhananjaya, B.L.; Shruthi, A. Synthesis, in vitro anthelmintic, and molecular docking studies of novel 5-nitro benzoxazole derivatives. *Med. Chem. Res.* **2015**, *24*, 1342–1350. [CrossRef]
47. Mickevičius, V.; Baltrušis, R.; Beresnevičius, Z. Synthesis and cyclization of N-(2-hydroxyphenyl)-β-alanines and N-(2-benzylhydroxyphenyl)-β-alanines. *Khim. Geterotsikl. Soedin.* **1991**, *4*, 527–531.
48. Clinical and Laboratory Standards Institute. *Performance Standards for Antimicrobial Susceptibility Testing; 24th Informational Supplement;* CLSI M100-S24; Clinical and Laboratory Standards Institute: Wayne, PA, USA, 2014.
49. Balouiri, M.; Sadiki, M.; Ibnsouda, S.K. Methods for in Vitro Evaluating Antimicrobial Activity: A Review. *J. Pharm. Anal.* **2016**, *6*, 71–79. [CrossRef]
50. Kurokawa, M.; Ying, B.W. Precise, High-throughput Analysis of Bacterial Growth. *J. Vis. Exp.* **2017**, *19*, 56197. [CrossRef]
51. Toh, S.C.; Lihan, S.; Bunya, S.R.; Leong, S.S. In Vitro Antimicrobial Efficacy of *Cassia alata* (Linn.) Leaves, Stem, and Root Extracts against Cellulitis Causative Agent *Staphylococcus aureus*. *BMC Complement. Med. Ther.* **2023**, *23*, 85. [CrossRef]
52. Adusei, E.B.A.; Adosraku, R.K.; Joppong-Kyekyeku, J.; Amengor, C.D.K.; Jibira, J. Resistance Modulation Action, Time-Kill Kinetics Assay, and Inhibition of Biofilm Formation Effects of Plumbagin from *Plumbago zeylanica* Linn. *J. Trop. Med.* **2019**, *2019*, 1250645. [CrossRef] [PubMed]
53. Mosmann, T. Rapid Colorimetric Assay for Cellular Growth and Survival: Application to Proliferation and Cytotoxicity Assays. *J. Immunol. Methods* **1983**, *65*, 55–63. [CrossRef] [PubMed]
54. Sheldrick, G.M. A short history of SHELX. *Acta Cryst.* **2008**, *A64*, 112–122. [CrossRef] [PubMed]
55. Bourhis, L.J.; Dolomanov, O.V.; Gildea, R.J.; Howard, J.A.K.; Puschmann, H. The anatomy of a comprehensive constrained, restrained refinement program for the modern computing environment—Olex2 dissected. *Acta Cryst.* **2015**, *A71*, 59–75.
56. Kiss, L.; Mándity, I.M.; Fülöp, F. Highly functionalized cyclic *β*-amino acid moieties as promising scaffolds in peptide research and drug design. *Amino Acids* **2017**, *49*, 1441–1455. [CrossRef]
57. Riaz, N.; Rehman, F.; Ahmad, M. *β*-Amino Acids: Role in Human Biology and Medicinal Chemistry—A Review. *Med. Chem.* **2017**, *7*, 302–307.
58. Šiugždaitė, J.; Lelešius, R.; Grybaitė, B.; Vaickelionienė, R.; Mickevičius, V. Synthesis and Biological Studies of New 2-Benzoxazolinone Derivatives as Antibacterial Agents. *Appl. Sci.* **2024**, *14*, 4783. [CrossRef]
59. Yadav, G.; Ganguly, S. Structure activity relationship (SAR) study of benzimidazole scaffold for different biological activities: A mini-review. *Eur. J. Med. Chem.* **2015**, *97*, 419–443. [CrossRef]
60. Jakubkiene, V.; Valiulis, G.E.; Schweipert, M.; Zubriene, A.; Matulis, D.; Meyer-Almes, F.-J.; Tumkevicius, S. Synthesis and HDAC inhibitory activity of pyrimidine-based hydroxamic acids. *Beilstein J. Org. Chem.* **2022**, *18*, 837–844. [CrossRef]
61. Kavaliauskas, P.; Grybaitė, B.; Sapijanskaite-Banevič, B.; Petraitienė, R.; Grigalevičiūtė, R.; Garcia, A.; Naing, E.; Mickevičius, V.; Belyakov, S.; Petraitis, V. Synthesis of novel N-substituted β-amino acid derivatives bearing 2-hydroxyphenyl moieties as promising antimicrobial candidates targeting multidrug-resistant Gram-positive pathogens. *PLoS ONE* **2025**, *20*, e0311715. [CrossRef]
62. Kavaliauskas, P.; Grybaitė, B.; Sapijanskaitė-Banevič, B.; Vaickelionienė, R.; Petraitis, V.; Petraitienė, R.; Naing, E.; Garcia, A.; Grigalevičiūtė, R.; Mickevičius, V. Synthesis of 3-((4-Hydroxyphenyl)amino)propanoic Acid Derivatives as Promising Scaffolds for the Development of Antimicrobial Candidates Targeting Multidrug-Resistant Bacterial and Fungal Pathogens. *Antibiotics* **2024**, *13*, 193. [CrossRef]
63. Kavaliauskas, P.; Acevedo, W.; Mickevičiūtė, E.; Grigalevičiūtė, R.; Grybaitė, B.; Sapijanskaitė-Banevič, B.; Pranaitytė, G.; Petraitis, V.; Petraitienė, R.; Mickevičius, V. 3,3′-((3-Hydroxyphenyl)azanediyl)dipropionic Acid Derivatives as a Promising Scaffold Against Drug-Resistant Pathogens and Chemotherapy-Resistant Cancer. *Pathogens* **2025**, *14*, 484. [CrossRef]
64. Yıldırım, M.; Ünver, H.; Necip, A.; Çimentepe, M. Design, synthesis, and biological evaluation of novel vanillin-derived hydrazone compounds with antimicrobial, anticancer, and enzyme inhibition activities, along with molecular structure and drug-likeness assessment. *Biochem. Biophys. Res. Commun.* **2025**, *775*, 152173. [CrossRef]
65. Nurkenov, O.A.; Fazylov, S.D.; Satpaeva Ž, B.; Seilkhanov, T.M.; Turdybekov, D.M.; Mendibayeva, A.Ž.h.; Kabieva, S.K.; Šulgau, Z.T.; Kulakov, I.V. Synthesis, structure and biological activity of hydrazones derived from 2- and 4-hydroxybenzoic acid hydrazides. *Chem. Data Collect.* **2023**, *48*, 101089. [CrossRef]

66. Adjissi, L.; Chafai, N.; Benbouguerra, K.; Kirouani, I.; Hellal, A.; Layaida, H.; Elkolli, M.; Bensouici, C.; Chafaa, S. New aromatic hydrazones: Synthesis, structural analysis, DFT study, biological activity, ADME-T properties and in silico evaluation of their inhibition of SAS-CoV-2 main protease. *J. Mol. Struct.* **2023**, *1279*, 134997. [CrossRef]
67. Greenwood, N.N.; Earnshaw, A. *Chemistry of the Elements*; Butterworth–Heinemann: Oxford, UK, 1997; pp. 800–804.
68. Didehdar, M.; Chegini, Z.; Tabaeian, S.P.; Razavi, S.; Shariati, A. Cinnamomum: The New Therapeutic Agents for Inhibition of Bacterial and Fungal Biofilm-Associated Infection. *Front. Cell. Infect. Microbiol.* **2022**, *12*, 930624. [CrossRef]
69. Baker, S.J.; Payne, D.J.; Rappuoli, R.; De Gregorio, E. Technologies to Address Antimicrobial Resistance. *Proc. Natl. Acad. Sci. USA* **2018**, *115*, 12887–12895. [CrossRef]